Chlorine partitioning between granitic melt and H2O-CO2-NaCl fluids in the Earth's upper crust and implications for magmatic-hydrothermal ore genesis

Journal Article

Author(s):
Hsu, Ying-Jui; Zajacz, Zoltán; Ulmer, Peter; Heinrich, Christoph A.

Publication date:
2019-09-15

Permanent link:
https://doi.org/10.3929/ethz-b-000356414

Originally published in:
Geochimica et Cosmochimica Acta 261, https://doi.org/10.1016/j.gca.2019.07.005

Accepted Manuscript

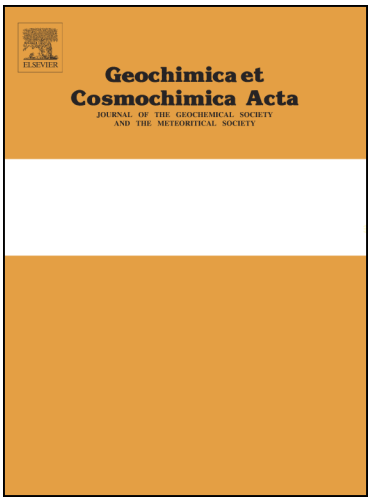

Chlorine partitioning between granitic melt and H_2O-CO_2-NaCl fluids in the Earth's upper crust and implications for magmatic-hydrothermal ore genesis

Ying-Jui Hsu, Zoltan Zajacz, Peter Ulmer, Christoph A. Heinrich

PII: S0016-7037(19)30415-6
DOI: https://doi.org/10.1016/j.gca.2019.07.005
Reference: GCA 11325

To appear in: *Geochimica et Cosmochimica Acta*

Received Date: 5 July 2018
Revised Date: 25 June 2019
Accepted Date: 1 July 2019

Please cite this article as: Hsu, Y-J., Zajacz, Z., Ulmer, P., Heinrich, C.A., Chlorine partitioning between granitic melt and H_2O-CO_2-NaCl fluids in the Earth's upper crust and implications for magmatic-hydrothermal ore genesis, *Geochimica et Cosmochimica Acta* (2019), doi: https://doi.org/10.1016/j.gca.2019.07.005

This is the Green Open Access version of the paper published in Geocheimica et Cosmochemica Acta (2019), v. 261, p. 171-190.

Chlorine partitioning between granitic melt and H_2O-CO_2-NaCl fluids in the Earth's upper crust and implications for magmatic-hydrothermal ore genesis

Ying-Jui Hsu[a,*,1], Zoltan Zajacz [a, b], Peter Ulmer [a], and Christoph A. Heinrich[a]

[a] Institute of Geochemistry and Petrology, ETH Zurich, Zurich, Switzerland

(Present e-mail address: ying-jui.hsu@umu.se)

[b] Department of Earth Sciences, University of Toronto, Toronto, ON, Canada

[*] Corresponding author.

[1] Present address: Department of Physics, Umeå University, Umeå, Sweden

Manuscript for revision 02 to *Geochimica et Cosmochimica Acta*

Abstract

Carbon dioxide is one of the most abundant volatile components in magmas after H_2O along with S and Cl, which are of great importance to the extraction of trace metals into magmatic-hydrothermal fluids and ore minerals. Yet the effect of CO_2 on the partition coefficients of chlorine between water-rich fluid and melt (i.e. the ratio of mass Cl concentrations in the corresponding phase; [$D^{fluid/melt}_{Cl}$]) is still poorly constrained. We conducted a set of experiments to constrain the effect of CO_2 on $D^{fluid/melt}_{Cl}$ by equilibrating felsic silicate melts with aqueous NaCl-bearing fluids while varying the concentration of CO_2 at pressures between 120 and 300 MPa and temperatures of 850 and 1000 °C. The starting melt was synthetized as a glass in the ternary albite-quartz-Al_2O_3 system to ensure the only significant metal chloride species in the equilibrium fluid phase was NaCl. The results demonstrate that $D^{fluid/melt}_{Cl}$ values increase with the concentration of Cl in the fluid phase and the silicate melt. The addition of CO_2 into aqueous metal chloride-bearing fluids induces a pronounced drop in $D^{fluid/melt}_{Cl}$, the extent of which is only weakly affected by pressure, temperature and fluid salinity, at least at relatively low Cl concentrations (<12 wt% NaCl equivalent). The values of $D^{fluid/melt}_{Cl}$ drop by approximately a factor of 3 in response to the addition of 20-25 mol% CO_2 to the fluid phase due to the decreased ability of the fluid to hydrate NaCl ion pairs. A new empirical equation describing wt%-based $D^{fluid/melt}_{Cl}$ is derived:

$$\mathbf{ln}[\mathbf{D}^{\mathbf{fluid/melt}}_{\mathbf{Cl}}] = 1.419(\pm 0.048) * \ln[\boldsymbol{P}] + 0.912(\pm 0.031) * \ln\left[\mathbf{C}^{\mathbf{fluid}}_{\mathbf{Cl}} + 1.434(\pm 0.260)\right] + \frac{4547(\pm 443)}{\boldsymbol{T}} - 4.026(\pm 0.155) * \mathbf{X}_{\mathbf{CO2}} - 9.790(\pm 0.440)$$

which expresses $D^{fluid/melt}_{Cl}$ as a function of pressure (in MPa), temperature (in Kelvins), and the equilibrium concentration of Cl (in wt%) and CO_2 (as molar fraction) in the fluid. The average absolute percentage error of the model predictions relative to the experimental data is 7.3%. The equation contains only monotonous functions to allow moderate extrapolation outside the range of

the calibration dataset as long as the fluid remains in the single-phase field (e.g. pressure above 100 MPa and up to 500 MPa or even higher). Our model equation represents a reasonable approximation for granitoid magma evolution in the upper and middle crust.

The presence of CO_2 suppresses fluid salinity at a given chloride content of a granitoid melt, which will also hinder the extraction of chloride-complexed ore metals (e.g. Cu, Pb, Zn, Mo, and Ag) into magmatic fluids, reducing the likelihood of base-metal ore formation (e.g. porphyry copper deposits) from such fluids in the uppermost crust. On the other hand, the highly volatile components, CO_2, H_2S and SO_2, are enriched in magmatic fluids exsolving early during the ascent of hydrous magmas. Chloride suppression by CO_2 and enrichment of fluids in sulfur species near the SO_2/H_2S predominance boundary favors extraction of sulfide-complexed metals, notably Au as $Au(HS)^0$, $Au(HS)_2^-$, $NaAu(HS)_2^0$ or $Au(HS)S_3^-$ into low-salinity magmatic fluids. Such fluids resemble those forming mid-crustal lode gold deposits that are typically poor in base metals. Our experimental results may therefore be taken as indirect support for a magmatic component in fluids forming orogenic lode gold deposits.

Key words: CO_2; chlorine; partitioning; C-O-H-Cl aqueous fluid; magma differentiation, volcanic degassing, ore deposit, copper, gold, hydrothermal, magmatic volatile phase

1. Introduction

Ascent of volatile-bearing magmas from depth to the surface or into the upper crust is a fundamental transport mechanism of volatile constituents such as H_2O, CO_2, S, and halogens on Earth. Chlorine is an important volatile element because of its role in the genesis of magmatic-hydrothermal ore deposits (e.g. Candela and Holland, 1984; Hedenquist and Lowenstern, 1994; Williams-Jones and Heinrich, 2005). Many ore metals form chloride complexes in high-temperature fluids, and therefore, the abundance of chloride in the fluid phase have a decisive effect on the efficiency of the extraction of metals from magmas and their transport to the sites of ore precipitation (Helgeson, 1969; Crerar and Barnes, 1976; Seward, 1981; Shinohara, 1994; Zajacz et al., 2008; Frank et al., 2011; Mei et al., 2014). Numerous experimental studies were conducted to determine the aqueous fluid/silicate melt partition coefficients of Cl [$D^{fluid/melt}_{Cl}$] representing the ratio of mass Cl concentrations in the corresponding phase over a wide range of pressure (*P*), temperature (*T*) and melt composition (Holland, 1972; Shinohara et al., 1989; Webster et al., 1999; Signorelli and Carroll, 2000; Signorelli and Carroll, 2002; Botcharnikov et al., 2004; Stelling et al., 2008; Webster et al., 2009; Zajacz et al., 2012; Webster et al., 2014; Botcharnikov et al., 2015). According to these studies, $D^{fluid/melt}_{Cl}$ increases with increasing pressure and increasing melt polymerization (i.e., higher $D^{fluid/melt}_{Cl}$ values were obtained in rhyolitic melts compared to basaltic melts). Chlorine is known to be dominantly present as NaCl, KCl, $FeCl_2$ and HCl in magmatic volatile phases, with HCl/metal chloride ratios increasing with decreasing pressure and increasing melt aluminosity; i.e. determined by A/CNK (=molar $Al_2O_3/(CaO + Na_2O + K_2O)$) (Holland, 1972; Chou and Eugster, 1977; Williams et al., 1997; Zajacz et al., 2012). The value of $D^{fluid/melt}_{Cl}$ varies as a function of Cl concentration due to the non-ideal behavior of dissolved aqueous metal chloride species (Webster, 1992a; b; Kravchuk and Keppler, 1994; Signorelli and Carroll, 2000; Signorelli and Carroll, 2002). The effect of temperature is not well constrained, whereas oxygen fugacity (fO_2) probably does not have a

significant effect on Cl partitioning over a range of fO_2 conditions from 1 log unit below to 4 log unit above the nickel – nickel oxide (NNO) buffer (Alletti et al., 2009; Shishkina et al., 2010; Zajacz et al., 2012; Beermann et al., 2015; Webster et al., 2015).

Carbon dioxide is commonly the second most abundant volatile component in magmas, which is expected to exert a pronounced effect on $D^{fluid/melt}_{Cl}$ because the addition of CO_2 into aqueous fluids decreases the capability of water to solvate polar or ionic solute species (e.g. Webster and Holloway, 1988). As a result, CO_2 significantly affects the mixing properties of H_2O-metal chloride fluids as well as vapor-liquid phase relationships (Joyce and Holloway, 1993; Duan et al., 1995; Shmulovich and Graham, 1999; Shmulovich and Graham, 2004). The addition of CO_2 to aqueous fluids lowers H_2O activity and the dielectric constant of the solvent, and therefore, decreases the stability of hydrated metal complexes, in particular electrically charged ones (Webster et al., 1989; Tattitch et al., 2015; Kokh et al., 2017). Despite its expected importance, only few experimental studies addressed the effect of CO_2 on $D^{fluid/melt}_{Cl}$ (Webster and Holloway, 1988; Botcharnikov et al., 2007; Alletti et al., 2009; Webster et al., 2015). These studies observed that $D^{fluid/melt}_{Cl}$ drops by approximately a factor of two in response to the addition of 20 mol% of CO_2 in relatively diluted fluid phases equilibrated with andesitic and basaltic melts (Botcharnikov et al., 2007; Alletti et al., 2009), whereas $D^{fluid/melt}_{Cl}$ seems unaffected by the addition of CO_2 to hypersaline fluids in equilibrium with basaltic and topaz rhyolite melts (Webster and Holloway, 1988; Webster et al., 2015). So far, no systematic investigation of the effect of CO_2 on $D^{fluid/melt}_{Cl}$ exists that simultaneously quantifies both the effect of CO_2 and total chloride concentration over a range of pressure and temperature.

In this study, we equilibrated slightly peraluminous albite-quartz (Ab-Qtz) melt with H_2O-CO_2-NaCl fluids (salinity < 25 wt% NaCl) and systematically varied CO_2 and NaCl concentrations at 120 - 300 MPa confining pressure and magmatic temperatures. The effect of CO_2, P, and T on $D^{fluid/melt}_{Cl}$

is quantified, and an empirical practical equation is provided that predicts $D^{fluid/melt}_{Cl}$ as a function of these variables for slightly peraluminous granitic melts.

2. Experimental and Analytical Methods

2.1. Experimental strategy

In this manuscript, the term "aqueous fluid" applies to the exsolving magmatic volatile phase of any density containing H_2O, salts and CO_2; the term "melt" refers to silicate melt and quenched run product glasses. To allow the physical-chemical interpretation, we synthetized our starting glass in the albite-quartz-Al_2O_3 system (i.e. K-free), which ensures that the only significant metal chloride species in the equilibrium fluid phase is NaCl, but the results will approximate natural haplogranitic magmas containing K in the melt and the fluid phase (Kravchuk and Keppler, 1994). The starting glasses are slightly peraluminous in composition, which is typical of arc granites (e.g. Grove et al., 2003; Nandedkar et al., 2014; Ulmer et al., 2018). The experiments were conducted at supercritical conditions in the H_2O-CO_2-NaCl system (i.e. in the single-phase field) to ensure that the activity-concentration relationship in the aqueous fluid was not affected by vapor-liquid immiscibility. Based on well-established data on the H_2O-NaCl fluid system (e.g. Bodnar et al., 1985; Driesner, 2007; Driesner and Heinrich, 2007), we selected the starting NaCl concentrations in the aqueous fluids so that they would fall into the single-phase field in the binary H_2O-NaCl system, with a large enough safety margin that they would likely remain a single phase even in the most CO_2-rich experiments at each specific *P-T* condition and not separate into brine and vapor. The critical pressure of the H_2O-NaCl system is approximately 170 MPa at 850 ^{o}C (Driesner and Heinrich, 2007); therefore we performed two sets of experiments at *P*=200 and 300 MPa. To address a broader range of pressures, and therefore fluid density, we also conducted a series of experiments at 120 MPa using starting

fluids with very low salinity to avoid brine saturation, which is predicted to occur at 3.3 wt% NaCl in the vapor in the pure H_2O-NaCl system. To address the effect of temperature, we repeated a part of the 200 MPa series at 1000 °C instead of 850 °C.

At each *P-T* condition, two complementary sets of experiments were conducted: one set with CO_2-free aqueous fluids with varying NaCl concentrations (X_{NaCl}= 0.005 to 0.16 at 300 and 200 MPa; 0.002 to 0.01 at 120 MPa), and another set with variable CO_2 mole fractions (X_{CO_2}) between 0 and 0.27 but with constant NaCl mole fraction in the volatile phase (i.e. X_{NaCl}=0.01 at 300 and 200 MPa and X_{NaCl}=0.002 at 120 MPa). In addition, experiments were conducted at higher X_{NaCl} values of 0.02 and 0.04 with X_{CO_2} of about 0.1 and 0.2 to evaluate if the relative effect of CO_2 on $D^{fluid/melt}_{Cl}$ is dependent on NaCl concentration in the low to intermediate salinity range. These additional experiments at elevated X_{NaCl} were mostly conducted at *T*=850 °C and *P*=200 MPa.

2.2. Starting materials

The composition of the starting glasses is in close approximation with the eutectic composition in the albite-quartz system at 200 MPa and a water activity of 1 (62 wt% Ab + 38 wt% Qz) with a slight excess of Al_2O_3 yielding an average A/NK (=molar $Al_2O3/(Na_2O+K_2O)$) of 1.060±0.019. The starting glass powders were prepared in two ways: (1) an anhydrous glass was synthetized from high-purity chemicals of SiO_2 (99.8%), aluminium oxide hydroxide (AlOOH), and Na_2CO_3 (99.95%). The reagents were thoroughly mixed in agate mortars under ethanol and the dried mixtures were dehydrated and decarbonated in a Pt crucible by slowly heating them up to 1000 °C overnight, and then fused in a high-T box furnace at 1600 °C for 40 mins. The crucible was covered by a lid during the fusing step to minimize alkali loss. The quenched glass was ground and remelted several times to ensure homogeneity. The loss of alkali was compensated by addition of minor amounts of Na_2CO_3

during remelting processes allowing to maintain nearly metaluminous compositions. The composition of the starting glass (GL6) was determined by electron microprobe and is shown in Table 1. (2) A hydrous starting glass was prepared from silica (SiO_2), aluminiumhyroxide ($Al(OH)_3$) and sodium metasilicate (Na_2SiO_3) powders. An aliquot of 200 mg of this mixture was placed into an $Au_{90}Pd_{10}$ capsule and welded shut. The capsule was run in a cold-seal pressure vessel at 1050 °C and 200 MPa for 5-6 hours and then quenched rapidly. The major element composition and homogeneity of the quenched glasses (HGL6-1, 6-3 and 6-5) were confirmed by electron microprobe analyses, as reported in Table 1. These two starting glasses represent equivalent compositions on anhydrous basis.

The starting solutions were prepared from high-purity chemicals and milli-Q water with varying NaCl concentrations and trace amounts (few hundreds ppm level) of other alkali-, and alkali earth chlorides (e.g., KCl, LiCl, RbCl, CsCl, $BaCl_2$, and $SrCl_2$). The added trace chloride concentrations are low enough that the total salt concentration in the fluid phase is present as NaCl component (>97%) in all experiments conducted at 300 and 200 MPa; only in the 120 MPa experiments, these added traces may contribute up to 15% of the total salt concentration due to the very low fluid salinity. Thus, NaCl is the major chloride component present in the system even in the relative low-pressure experiments. Anhydrous oxalic acid ($H_2C_2O_4$; ≥ 99%) was loaded in the capsules as a CO_2 source for the CO_2-bearing experiments. All chemicals were dried at 110 °C in an oven overnight before use.

2.3. Experimental techniques

The experiments were conducted in rapid-quench Molybdenum-Hafnium Carbide (MHC) cold-seal pressure vessels at 850 – 1000 °C and 120 – 300 MPa at ETH Zurich. The vessel setup consists of the MHC vessel, a water-cooled coupling and a cold steel extension vessel. Temperature was monitored with K-type thermocouples that are fixed to the outside of the vessel, and these were cross

calibrated with an internal thermocouple to allow precise and accurate *T* determination in actual experiments for which internal thermocouples cannot be applied as they would prevent rapid quenching. The temperature gradient was <10 °C over 20 mm length and the overall accuracy of temperature determination is thought to be better than ±5 °C. Argon was used as pressure medium and the pressure during the experiment were maintained within ± 5 MPa of the nominal value. As the furnace-vessel assembly allows 180 degree rotation, the capsule was dropped into the cold steel extension for rapid quenching by rotating the vessel into vertical position (i.e. the melt reached the glass transition temperature within seconds). Due to the small temperature gradient in the vessel, and small capsule sizes (3x10 mm), 3 to 4 capsules could be run in a single experiment, with two capsules placed side by side.

The starting glass (5-7 mg) was placed into an Au capsule (3 mm OD, 2.75 mm ID). Large glass fragments, up to a few hundred microns in diameter, were loaded into the capsules to avoid the formation of bubbles within the melt which may not escape during the experiment due to high melt viscosity (Behrens et al., 2004). The starting solution (5-7 µL) with varying Cl concentrations and various amounts of anhydrous oxalic acid was then loaded into the capsule, depending on the desired CO_2/H_2O ratio in the aqueous fluid phase. The decomposition of oxalic acid ultimately leads to the generation of CO_2 and H_2 at run conditions, but H_2 is rapidly lost from the capsule by diffusion until fH_2 inside the capsule and in external pressure medium becomes equal. After loading, the capsules were crimped and carefully welded with a PUK 3 Professional welder to avoid any volatile loss. The weight of the capsule before and after welding was compared and the capsule was only used if the weight difference did not exceed 2% of the mass of the loaded solution. After welding, the capsules were placed into a 110 °C furnace for at least 12 h and then weighed again to confirm their integrity. After the high-pressure experiment, they were weighed again to confirm the absence of leakage. For all experiments, we applied a relatively high fluid to melt mass ratio of 0.9 – 1.5 in order to allow

obtaining the composition of the aqueous fluid phase by mass balance precisely (Zajacz et al., 2012). As the hydrogen fugacity in the Ar pressure medium was very low (nominally <0.01 bars, 99.996% purity Ar used), and the water activity in the capsule was high, the oxygen fugacity in these experiments was high enough to avoid the formation of reduced C-species (i.e. CO or CH_4) in the fluid phase above trace concentration level (Chou, 1987). Model calculations using hydrogen permeability coefficients for Au from Chou (1987) suggest that hydrogen produced by oxalic acid decomposition is effectively lost from the capsule in less than 2 hours even in the most CO_2-rich case from our experimental series. Tattitch et al. (2015) confirmed the lack of any significant C species in the fluid other than CO_2 by Raman spectroscopy on synthetic fluid inclusions produced in experiments with up to 45 mol% CO_2 added as oxalic acid, which were run at even lower *T* (800 ^{o}C), for similar durations and using similar capsule material ($Au_{94}Cu_6$ alloy). The starting compositions and experimental run conditions are summarized in Table 2 and 3.

2.4. Analytical techniques

The glass compositions before and after the experiment were analyzed by a JEOL JXA-8200 electron microprobe at 15 kV accelerating voltage. A 20 μm diameter defocused beam was used to reduce element migration under the electron beam. In addition, analyses of major elements (Si, Al, Na and K) were performed with a low, 5-7 nA, beam current to avoid Na and K loss; whereas chlorine concentrations were analyzed with 50-60 nA beam current to improve the signal to noise ratio. For Si and Al, the Smithsonian VG A-99 basalt glass-standard was used whereas albite and K-feldspar standards were used for Na and K, respectively. An in-house scapolite standard containing 1.83 wt% Cl was employed as standard for chlorine analyses. The counting times were the following: 20 s peak and 10+10 s background for major elements, 60 s peak and 30 + 30 s background for Cl. The accuracy of major element analysis was checked by routinely measuring the Smithsonian VG A-

568 rhyolite glass standard as a secondary standard. For Cl analysis, the scapolite standard was measured as an unknown sample regularly yielding long-term accuracy of 1.2 relative %. The detection limit for major elements and Cl was estimated to be 0.01 wt%.

2.5. Mass balance calculations

The concentrations of Cl in the aqueous fluid phase at run conditions were determined by mass balance calculations. The composition of the aqueous fluid phase is calculated from the measured starting and run product glass compositions and the known composition of the starting solutions, assuming that the change in the composition of the glass is only due to element redistribution between the melt and the aqueous fluid phase (Zajacz et al., 2012). The following mass balance equation was used to derive the composition of the fluid phase at run conditions:

$$m_{aq\_0} \times C_{Cl}^{aq\_0} + m_{gl\_0} \times C_{Cl}^{gl\_0} = m_{aq\_P} \times C_{Cl}^{aq\_P} + m_{gl\_P} \times C_{Cl}^{gl\_P} \quad (1)$$

where m is the mass of a specific phase, and C_{Cl} is the concentration of Cl in the indicated phase. Subscript aq_0 and gl_0 denote the starting solution and the starting glass, respectively; whereas subscript aq_P and gl_P refer to the run product aqueous fluid and glass phases, respectively. Note that the EPMA totals are systematically 1-2 wt% lower than expected based on the estimated dissolved water and CO_2 concentrations (Table S1 and S2). We therefore calculated volatile (H_2O and CO_2) concentrations in the run product glass based on the solubility model of Papale et al. (2006). We further assumed that the mass of the silicate melt is only affected during the experiment by the dissolution of volatile components (H_2O, CO_2 and Cl) into the molten starting glass for anhydrous starting glass (GL-6); for the hydrous starting glass (HGL6, HGL6-3 and HGL6-5), the difference between the starting and the predicted equilibrium water concentration was considered. The uncertainties on the starting and run product glass compositions were propagated into the calculated

equilibrium fluid compositions. Due to the high fluid/melt mass ratio, the error resulting from the uncertainty on the water concentration in the silicate melt has a negligible effect on the estimated mass of the fluid phase at run *P-T.* Similarly, the uncertainty on the measured Cl concentration in the glass phase has negligible effect on the estimated Cl concentration in the fluid phase. The propagated error on the mass balance-calculated Cl concentration in the fluid phase at run conditions is estimated to be less than 2 % relative for all experiments (see error modeling in Fig. 1 of Zajacz et al., 2012).

The Cl partition coefficient between aqueous fluid and silicate melt phase was calculated as:

$$D^{fluid/melt}_{Cl} = \frac{C^{aq}_{Cl}{}^{P}}{C^{gl}_{Cl}{}^{P}} \qquad (2)$$

Where $C^{aq}_{Cl}{}^{P}$ and $C^{gl}_{Cl}{}^{P}$ are Cl concentrations (in ppm) in aqueous fluid and melt phases, respectively. Error propagation was also applied here to yield the final uncertainty (1 σ) on $D^{fluid/melt}_{Cl}$.

3. Results

3.1. Experimental run product glass compositions

The compositions of the run product glasses are provided in Supplementary Table S1 and S2. In all experiments, the run product glasses are devoid of any crystals. Experiments conducted with hydrous starting glass generally contain vesicles ranging from <1 to 100 μm in diameter (Fig. 1b) whereas the run products of experiments conducted with anhydrous starting material are bubble-free (Fig. 1a). Even in the bubble-bearing glasses, the volume of the bubbles is small relative to the volume of the melt phase, which enabled us to avoid them during analytical work. All bubbles are thought to have been a stable fluid phase at run conditions, which could not physically separate from the melt due to its high viscosity. The presence of only salt precipitate-free bubbles with seemingly uniform density (Fig. 1c) is an additional evidence showing that the fluids remained in the single-

phase field at the experimental run conditions. An exception is experiment #57c in which the fluid contained 16 mol% NaCl (i.e. 38 wt% NaCl), which is above the solubility of NaCl in water at ambient temperature, and thus NaCl nucleated in the bubbles in the glass upon quenching (Fig. 1d).

The major element composition of the run product glasses only showed slight modification compared to the starting glasses after normalization to an anhydrous basis. Their compositions were slightly peraluminous except very few which are slightly peralkaline, with molar A/NK, ratios of 0.978-1.128 (Table 2 and 3), similar to the starting glasses (average A/NK=1.060±0.019). Because H_2O is the dominant phase in the aqueous fluid (i.e. X_{H_2O}= 0.84-0.998) and most experiments contained either supercritical or vapor-like fluids, the increase of Cl concentration in the aqueous fluid (=C_{Cl}^{fluid}) is not expected to affect dissolved water concentrations significantly as was shown by numerous previous studies (Webster, 1997; Webster et al., 1999). However, the addition of CO_2 into the system significantly decreases the amount of H_2O dissolved in the silicate melt. At a given constant Cl concentration in the initial fluid (i.e. constant X_{NaCl}), the estimated H_2O contents based on difference of EPMA totals were 1.1-2.3 wt% lower with 24 mol% of CO_2 in the fluid than the estimated H_2O contents from the CO_2-free experiments.

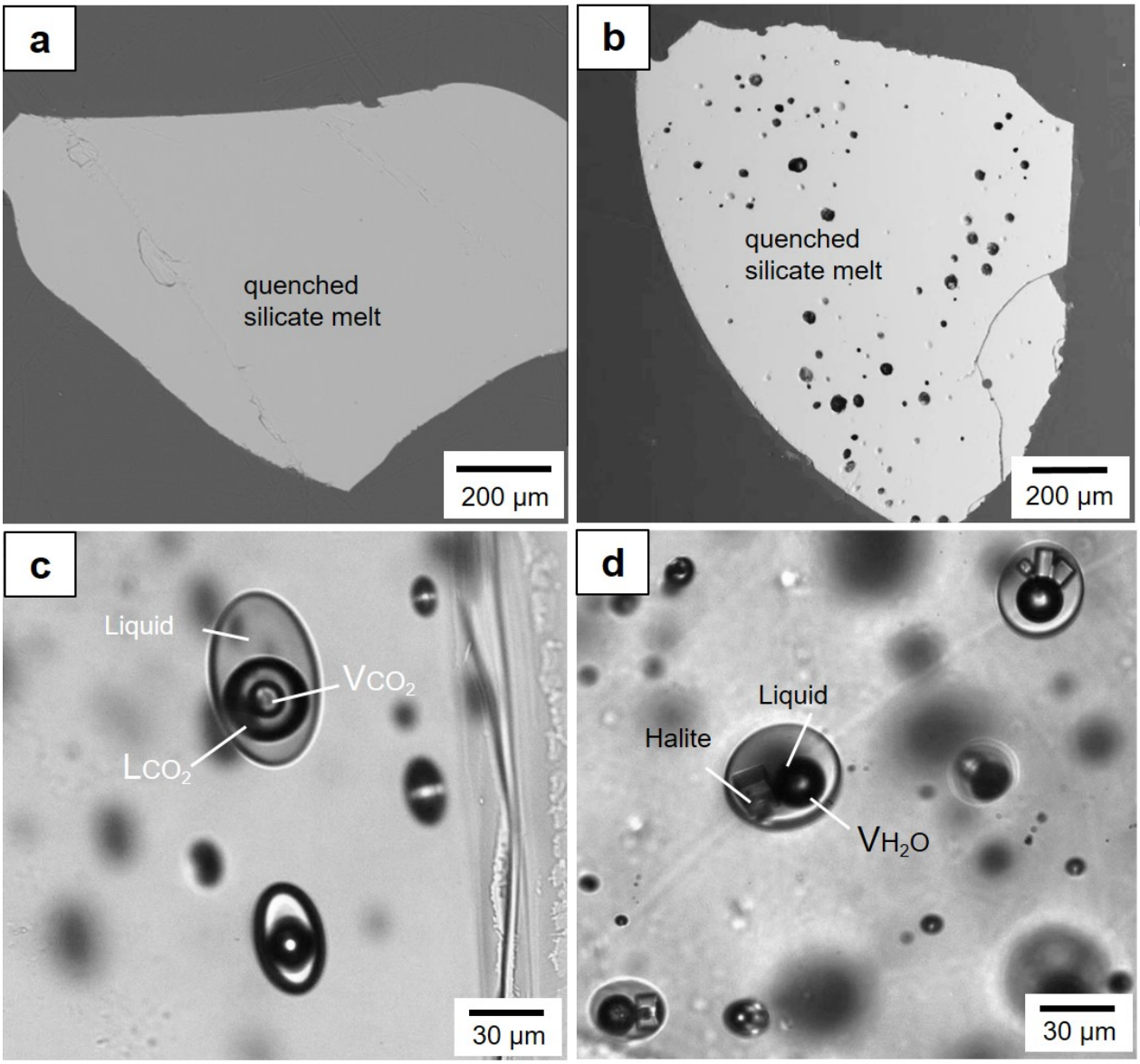

Fig. 1 Photomicrographs of experimental run product glasses and representative fluid inclusions. **(a)** Back-scattered electron (BSE) image of the run product glass from experiment #65a, a typical example of experiments conducted with anhydrous starting glass (GL6). The experiment was performed at 300 MPa, 850 °C with the initial fluid composition containing 1 mol% NaCl. **(b)** BSE image of the run product glass from experiment #64a, conducted with the hydrous starting glass of HGL6-3 containing about 4 wt% H_2O initially. The experiment was performed at 120 MPa, 850 °C with the initial fluid composition containing X_{NaCl}=0.16 and X_{CO_2}=0.14. **(c)** CO_2-rich fluid inclusions in run product glass from experiment #11c conducted at 300 MPa and 850 °C. The inclusions consist of liquid and vapor CO_2 bubbles coexisting with and aqueous liquid phase. **(d)** Fluid inclusions in run product glass of a high-NaCl experiment (#57c, X_{NaCl}=0.16) at 200MPa, 850

°C. All inclusions contain halite crystals corresponding to fluid salinities above the room-temperature solubility of NaCl in water.

3.2. Achievement of equilibrium

The homogeneity of the run product glasses with respect to all element concentrations including Cl is an evidence for close approach to equilibrium as the silicate melt is the phase characterized by the lowest element diffusivities within the capsule. The high water concentrations in the silicate melts in our experiments likely promoted the rapid achievement of equilibrium by increasing element diffusivities, and so did the small amount of loaded glass by reducing the required diffusion lengths. In addition to paying attention to the homogeneity of each run product glass with respect to slowly diffusing elements, in particular Cl, we conducted time-series experiments with run durations of 24, 48 and 94 h at 200 MPa and 850 °C. For these, an aqueous fluid with 1 mol% NaCl and 8 mol% CO_2 was equilibrated with the Cl-free starting glasses. The Cl concentration was analyzed by EPMA in the run product glasses along core to rim profiles. The results showed that chlorine was distributed heterogeneously (1 sigma ~10 relative %) in the run product glass from 24 h experiment but was homogeneous (1 sigma < 2 relative %) in the 48 and 94 h runs. The value of $D^{fluid/melt}_{Cl}$ derived from the 24 h experiment is correspondingly higher than those derived from the 48 and 94 h experiments due to the lower average Cl concentration in the glass. The latter two experiments yielded nearly identical $D^{fluid/melt}_{Cl}$ testifying that equilibrium was attained in less than 48 h (Fig. 2). Therefore, run durations of at least 48 - 60 h were used in the subsequent experiments. Additionally, for some CO_2-rich experiments at 120 MPa, we conducted experiments for 96 to 168 h because of slower Cl diffusivities in the melt resulting from the lower dissolved H_2O concentrations. These run durations were sufficient to produce a homogeneous glass even at 120 MPa.

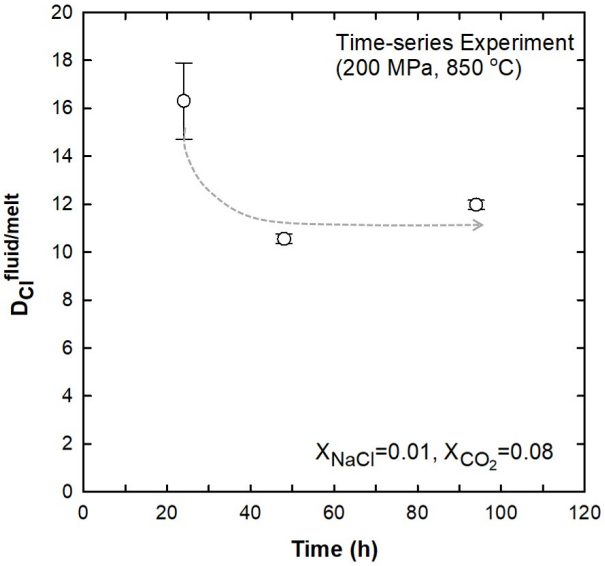

Fig. 2 $D_{Cl}^{fluid/melt}$ as a function of run duration from time-series experiments performed at 200 MPa and 850 °C. The higher $D_{Cl}^{fluid/melt}$ observed in the 24 h experiment is consistent with the fact that Cl did not have sufficient time to attain equilibrium concentrations in the inner parts of the melt bead by diffusing in from the fluid phase. The run product glasses from the 48 and 96 h experiments were homogeneous with respect to Cl (and all other elements) and yielded consistent $D_{Cl}^{fluid/melt}$ with very low uncertainty testifying attainment of equilibrium in less than 48 h.

3.3. The partitioning of Cl between aqueous fluid and melt

3.3.1. CO_2-free system

The Cl concentrations in the equilibrated silicate melt increase non-linearly with the increase of total chloride concentration (i.e. X_{NaCl}=0.002 – 0.16) while *P* and *T* is held constant (Fig. 3a). At *T*=850 °C, while X_{NaCl} in the starting fluid increases from 0.002 to 0.16, the dissolved Cl in the melt increases from 315 to 1206 ppm at *P*=300 MPa, from 743 to 2130 ppm at P=200 MPa, and from 702 to 2518 ppm at *P*=120 MPa. At *P*=200 MPa and *T*=1000 °C, the Cl concentration in the melt shows significant increase from 969 to 2569 ppm as X_{NaCl} in the fluid increases from 0.005 to 0.02, whereas it shows a slight drop to 2139 ppm as X_{NaCl} increases from 0.02 to 0.04 (Fig. 3a). This

slight drop of the Cl concentration in the melt may relate to extreme non-ideal behavior in the H_2O-NaCl fluid phase at near critical conditions (Driesner and Heinrich, 2007).

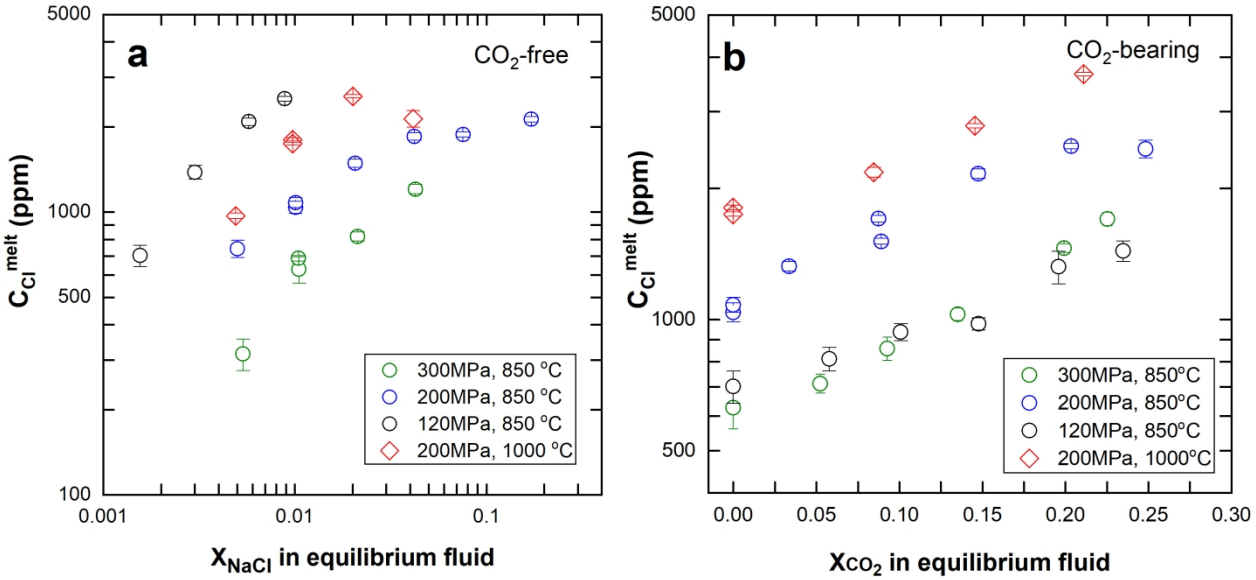

Fig. 3 Concentration of Cl in the silicate melt and co-existing equilibrium H_2O-Cl and H_2O-Cl-CO_2 aqueous fluids at *P*=120, 200 and 300 MPa and *T*=850 and 1000 °C. Aqueous fluid compositions were calculated by mass balance calculations (see details in text and also in Table 2 and 3). (a) In the CO_2-free system, Cl concentration in the melt increases with decreasing *P*, increasing *T* and increasing total chloride concentration in the aqueous fluids. (b) In the CO_2-bearing system, Cl concentration in the melt significantly increases with increasing CO_2 concentration in the aqueous fluids at constant chlorine concentration in the fluid (X_{NaCl}=0.012 at 200 and 300 MPa, and X_{NaCl} =0.002 at 120 MPa).

Our data reveal that $D^{fluid/melt}_{Cl}$ increases with increasing concentrations of Cl in the melt (=C^{melt}_{Cl}) and the aqueous fluid (=C^{fluid}_{Cl}) in the CO_2-free system at the run *P*-*T* conditions. At *T*=850 °C, with increasing $X_{NaCl\,(equiv.)}$ in the system, $D^{fluid/melt}_{Cl}$ increases from 30.0 to 64.8 (X_{NaCl} = 0.005 - 0.04) at 300 MPa; from 13.5 to 114.6 (X_{NaCl} = 0.005 - 0.17) at 200 MPa; and from 5.3 to 8.2 (X_{NaCl} = 0.002 - 0.009) at 120 MPa (Table 2). At nearly identical Cl concentration of X_{NaCl} =0.01 in the

aqueous fluid, the value of $D^{fluid/melt}_{Cl}$ increased approximately by a factor of 4 from 8.2 at *P*=120 MPa to 33.0 at 300 MPa. Whereas, at *T*=1000 °C and X_{NaCl}= 0.005 – 0.04, the value of $D^{fluid/melt}_{Cl}$ increases from 10.1 to 35.7 at 200 MPa (Table 2).

3.3.2. CO_2-bearing system

In the CO_2-bearing system, the general observation is that C^{melt}_{Cl} increases with increasing concentration of CO_2 in the equilibrium fluids while X_{NaCl} in the fluid is held nearly constant (Fig. 3b). Accordingly, the value of $D^{fluid/melt}_{Cl}$ decreases in a non-linear manner with increasing CO_2 concentration in the fluid: at a constant X_{NaCl} of ~0.012, while raising X_{CO_2} from 0 to 0.25, the value of $D^{fluid/melt}_{Cl}$ decreases from 33.0 to 11.3 at *P*=300 MPa and from 19.2 to 7.1 at *P*=200 MPa; whereas at a constant X_{NaCl} of 0.002 at 120 MPa, $D^{fluid/melt}_{Cl}$ decreases from 5.4 to 1.9 within the same range of X_{CO_2}. At *T*=1000 °C and a constant X_{NaCl} of ~0.012, $D^{fluid/melt}_{Cl}$ decreases from 10.7 to 5.0 as X_{CO_2} increases from 0 to 0.21 (Table 3). Therefore, it is apparent that $D^{fluid/melt}_{Cl}$ decreases by about a factor of 3 in response to the addition of about 24 mol% CO_2 to the fluid phase at *P*=120-300 MPa and at *T*=850 °C, and this effect is independent of the confining pressure, at least between 120 and 300 MPa. Additional experiments conducted at X_{NaCl}=0.02 and 0.04 at *P*=200 MPa showed that the addition of ~10 mol% CO_2 to the fluid reduces $D^{fluid/melt}_{Cl}$ by a factor of 1.5, i.e. to a similar extent to that observed at lower NaCl concentration. Experiments #77a and #78a with X_{CO_2} of 0.2 and 0.25 yielded identical Cl concentrations in the melt for X_{NaCl} (fluid)=0.019 and 0.042, indicating that these experiments must have entered the vapor-liquid immiscibility field, otherwise the Cl concentration in the melt should be higher in equilibrium with the more NaCl-rich fluid. To check at what fluid salinity the vapor limb of the solvus is located at X_{CO_2} ~0.2, we conducted an additional experiment with X_{NaCl} (fluid)=0.015 (experiment #73a). The experiment yielded

identical Cl concentration in melt to those at X_{NaCl} (fluid)=0.019 and 0.042, but higher than that with X_{NaCl} (fluid)=0.012, thus the vapor limb of the solvus is confined between X_{NaCl} (fluid)=0.012 and 0.015 at X_{CO_2}(fluid)~0.2. As the critical pressure of the H_2O-NaCl system at *T*=850 °C is only about 170 MPa, the above observation suggests that the addition of CO_2 greatly expands the vapor-liquid immiscibility field consistent with previous studies (Frantz et al., 1992; Shmulovich and Graham, 1999; Shmulovich and Graham, 2004). With similar logic, we concluded that experiment #81c at *T*=1000 °C must have also been located in the vapor-liquid immiscibility field. Apart from this, the effect of CO_2 is slightly smaller at 1000 °C, as $D^{fluid/melt}_{Cl}$ decreases only by a factor of 2 as X_{CO_2} increases from 0 to 0.21. As mass balance calculation cannot be applied to derive the composition of the fluid phase in experiments containing both vapor and liquid, no $D^{fluid/melt}_{Cl}$ were calculated for all the above listed experiments falling into the vapor-liquid immiscibility field.

Another notable observation is that the maximum dissolved Cl concentration in the melt increases with CO_2 addition to the fluid. For example, at *T*=850 °C and *P*=200 MPa, the CO_2-free fluid reaches a plateau of maximum Cl concentrations in the melt around 2100 ppm (i.e. at X_{NaCl} of 0.04-0.17; Fig. 3a), whereas the vapor-liquid saturated experiments at X_{CO_2}~0.2 exhibit C^{melt}_{Cl}=2753 ppm (Fig. 3b). This effect is even more pronounced at *T*=1000 °C, where the maximum observed C^{melt}_{Cl} amounts to 2569 ppm in the CO_2-free system as opposed to 4012 ppm in the CO_2-bearing system at X_{CO_2}=0.22 (Fig. 3a and b).

4. Discussion

4.1. Chlorine speciation in the aqueous fluid

For the selected starting glass composition in the Ab-Qtz-Al_2O_3 system, the only major chloride component in the fluid phase is NaCl and possibly some minor HCl (Holland, 1972; Williams et al., 1997; Shinohara, 2009). Note that the true speciation of NaCl and HCl is likely more complicated as it may involve partial dissociation to ions at higher fluid densities, and the formation of NaCl ion pair clusters at high NaCl concentrations (Driesner et al., 1998). Nevertheless, for our purposes, it is more practical to treat NaCl and HCl as thermodynamic components without taking true speciation into account. Because the concentrations of Na_2O in the run product glasses are nearly unchanged (average 7.53 ± 0.42 wt% in anhydrous basis) compared to the starting composition and thus the A/NK of the silicate melt did not decrease significantly, it is likely that the fluids remained NaCl dominated at all conditions. Indeed, we calculated the HCl/NaCl ratio in the fluid (Table 2 and 3), assuming that all Na was gained or lost (by mass) by the glass via the following exchange reaction between the silicate melt and fluid phases:

$$2\mathrm{NaCl}_{(aq)} + \mathrm{H_2O}_{(m)} = \mathrm{Na_2O}_{(m)} + 2\mathrm{HCl}_{(aq)} \quad (3)$$

Where "(aq)" and "(m)" denotes components in the aqueous fluid and the silicate melt phase, respectively. Unfortunately, the propagated error on the such derived HCl/NaCl ratios is rather large, in particular for experiments in which the Cl concentration in the fluid was very low, such as those at 120 MPa. However, those with higher Cl in the fluid and thus reasonable uncertainties (i.e. <0.2 absolute error) yielded systematically low HCl/NaCl values below 0.2. This observation is in accord with Shinohara (2009) concluding that the HCl-NaCl exchange reaction between silicate melt and aqueous fluid is strongly pressure dependent, and NaCl-rich fluids are dominant at P >50 MPa in magmatic aqueous fluids. The data of Williams et al. (1997) would predict higher HCl/NaCl ratios for most of our fluids, however, their Na-H exchange coefficients were obtained at lower *P*, namely 50 and 100 MPa, and they have also shown that the relative abundance of HCl decreases with increasing pressure. Sodium chloride is likely the dominant chloride species in the silicate melt as

well in our experiments, because Na is the only available network-modifier cation to complex with Cl. Therefore, the partitioning of NaCl between aqueous fluid and silicate melt at our run conditions is dominantly controlled by the following reaction:

$$NaCl_{(aq)} = NaCl_{(m)} \quad (4)$$

4.2. The effect of Cl concentration and temperature on $D^{fluid/melt}_{Cl}$

At identical pressure, the increasing $D^{fluid/melt}_{Cl}$ with increasing Cl concentration may be due to non-ideal behavior of chloride species in the silicate melt and/or the aqueous fluid phase as observed in our experiments from both CO_2-free and CO_2-bearing systems (Fig. 3 and 4). Shinohara et al. (1989) assumed that the mixing of chloride with silicate melt may obey Henry's law, and the variation of the $D^{fluid/melt}_{Cl}$ was attributed to variation in the activity coefficients of major chloride species in supercritical fluids. Kravchuk and Keppler (1994) computed the activity coefficients of $NaCl^0$ species in the H_2O-NaCl system at 800 ^oC and 200 MPa using the equation of state of Anderko and Pitzer, (1993). The positive correlation between $D^{fluid/melt}_{Cl}$ and C^{fluid}_{Cl} was explained by the decreasing activity coefficient of dissolved chloride species in the aqueous fluid phase with increasing C^{fluid}_{Cl}.

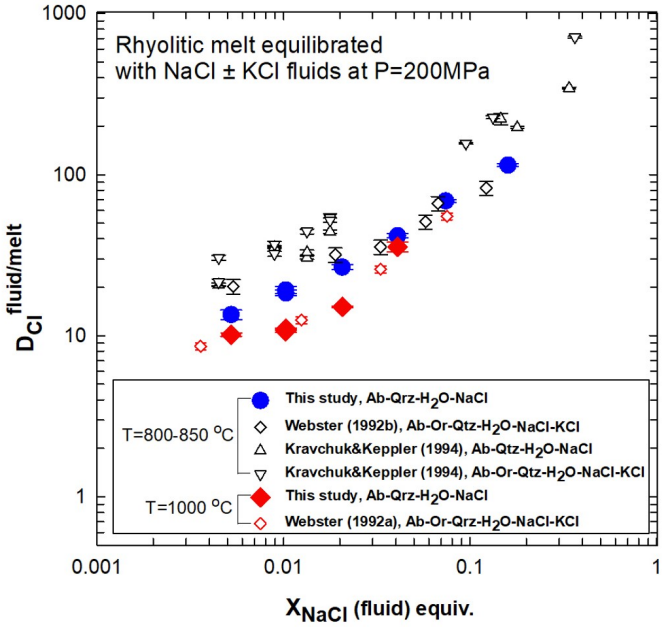

Fig. 4 $D^{fluid/melt}_{Cl}$ as a function of equivalent NaCl molar fraction (i.e. $X_{NaCl(equiv.)}$(fluid) =(nNaCl+nKCl)/(nNaCl+nKCl+nH_2O) where n is number of moles of each component) in the equilibrium aqueous fluid at *P*=200 MPa. For comparison, experimental data conducted on rhyolitic melt compositions with A/NK~1 at *T*=800-850 °C (blue and black symbols) and 1000 °C (red symbols) are shown. Temperature has slightly negative effect on the values of $D^{fluid/melt}_{Cl}$ as *T* increases from 850 to 1000 °C, consistent with the study of (Webster, 1992a).

Increasing $D^{fluid/melt}_{Cl}$ with increasing concentration of Cl in a similar coexisting aqueous fluid has been observed in several studies for a wide range of melt compositions (Webster and Holloway, 1988; Shinohara et al., 1989; Kravchuk and Keppler, 1994; Webster et al., 1999; Signorelli and Carroll, 2000; Stelling et al., 2008). However, $D^{fluid/melt}_{Cl}$ is also strongly influenced by the melt composition. The dissolved Cl concentrations in basaltic melts can be more than an order of magnitude higher than in rhyolitic melts (Shinohara et al., 1989; Webster et al., 1999; Webster and De Vivo, 2002; Mathez and Webster, 2005; Stelling et al., 2008; Webster et al., 2015). When considering rhyolitic melts, Cl is less strongly partitioned in favor of the fluid phase if the melt

composition is peralkaline or peraluminous rather than metaluminous (i.e. A/NK=1) (Metrich and Rutherford, 1992; Webster and De Vivo, 2002). Therefore, we restrict the comparison of our data with other experimental data to haplogranite melt with composition of A/NK~1 at nearly identical pressure and temperature conditions. It is apparent in Figure 4 that at *P*=200 MPa and *T*=800-850 °C where all experiments contained supercritical fluids, the $D^{fluid/melt}_{Cl}$ vs. C^{fluid}_{Cl} slope is nearly identical over a significant range of NaCl ± KCl concentrations in the aqueous fluid (equivalent X_{NaCl} =0.004 – 0.36) as reported by previous studies (Webster, 1992b; Kravchuk and Keppler, 1994). Furthermore, the observation that $D^{fluid/melt}_{Cl}$ slightly decreases while *T* increases from 850 to 1000 °C is in good agreement with the finding of Webster (1992a) at *P*=200 MPa and *T*=1000 °C for haplogranite melt compositions (Fig. 4). Importantly, the data on Figure 4 also clearly demonstrates that there is no significant difference between $D^{fluid/melt}_{Cl}$ in the Ab-Qtz (±Al_2O_3) and Ab-Qtz-Or (±Al_2O_3) systems, i.e. replacement of a part of Na by K does not affect Cl partitioning noticeably. By extension, this means that the data and model equations presented in this study also apply to true haplogranitic melt compositions as long as they are metaluminous to slightly peraluminous.

4.3 The effect of pressure on $D^{fluid/melt}_{Cl}$

The observed increase of $D^{fluid/melt}_{Cl}$ with increasing pressure in both CO_2-free and CO_2-bearing systems (Fig. 5 and 6a) can be explained by the decreasing activity coefficients of NaCl $_{(aq)}$ with increasing fluid densities and also increasing dissociation of NaCl ion pairs into Na^+ and Cl^-. This is expected, because the ability of water to hydrate the strong dipole NaCl ion pairs is higher at higher fluid densities due to the increased dielectric constant of water (Helgeson, 1981; Bowers and Helgeson, 1983; Driesner et al., 1998). A similar correlation between pressure and $D^{fluid/melt}_{Cl}$ was observed by Shinohara et al. (1989) who systematically investigated the partitioning of Cl between haplogranite melts and aqueous fluids. With an identical fluid concentration of about X_{NaCl}=0.01 in

the initial fluid, the $D_{Cl}^{fluid/melt}$ increased from ~15 at *P*=120 MPa up to ~550 at *P*=600 MPa, in good accordance with our data (Fig. 5). Webster (1992a) also reported $D_{Cl}^{fluid/melt}$ increasing from 22 at *P*=200 MPa up to 177 at *P*=800 MPa at a total Cl concentration of ~0.5 molal (i.e. X_{NaCl}=0.01) in the fluid. Signorelli and Carroll (2000) observed a similar pressure effect on $D_{Cl}^{fluid/melt}$ in a phonolite melt – aqueous fluid system. This positive effect of pressure on $D_{Cl}^{fluid/melt}$ has been interpreted as a consequence of the large negative partial molar volume of NaCl in the fluid phase (Shinohara et al., 1989; Signorelli and Carroll, 2002; Dolejš and Zajacz, 2018).

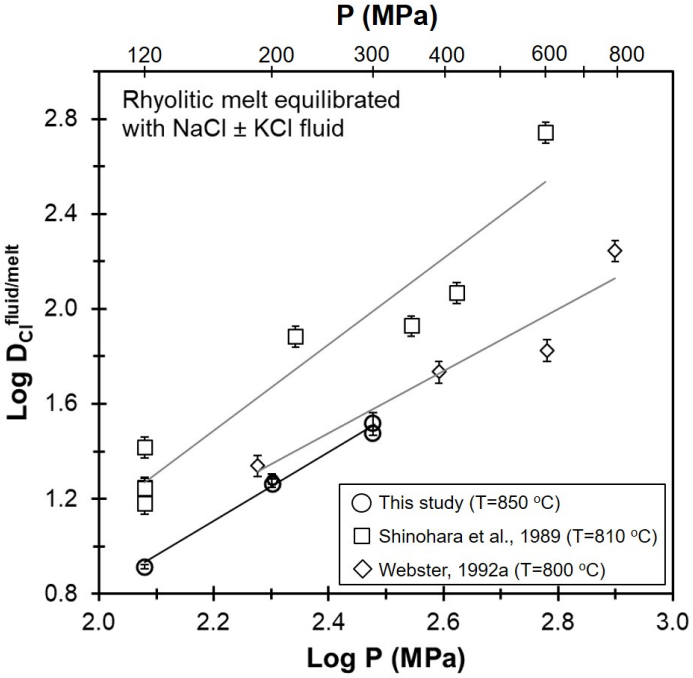

Fig. 5 Logarithmic diagram displaying the pressure dependence of $D_{Cl}^{fluid/melt}$ in low-salinity aqueous fluids equilibrated with rhyolitic melts at *P*= 120 – 800 MPa. The initial fluid composition contained NaCl ± KCl concentrations of approximately 0.4 – 0.6 molal from this study and other studies (i.e. X_{NaCl}≈0.01). A positive linear correlation between the logarithms of $D_{Cl}^{fluid/melt}$ and pressure is observed: y=1.45(±0.11)*x-2.09(±0.22), R^2=0.989 (this study); y=1.81(±0.16)*x-2.49(±0.47), R^2=0.922 (Shinohara et al., 1989); y=1.31(±0.23)*x-1.66(±0.50), R^2=0.913 (Webster, 1992a). Shinohara et al. (1989) used an eutectic melt composition in the Ab-Or-Qtz-H_2O system at 500 MPa and aH_2O=1, and Webster (1992a) studied Ab-Or-Qtz mixtures with peraluminous compositions.

4.4 The effect of CO_2 on $D^{fluid/melt}_{Cl}$

As mentioned above, Cl is present as NaCl in both aqueous fluid and silicate melt, and thus we can derive the thermodynamic equilibrium constant for Eq (4):

$$K_4 = \frac{a^{aq}_{NaCl}}{a^{m}_{NaCl}} = \frac{C^{aq}_{NaCl}}{C^{m}_{NaCl}} \times \frac{\gamma^{aq}_{NaCl}}{\gamma^{m}_{NaCl}} \qquad (5)$$

where K_4 is the equilibrium constant of Eq. (4), a is activity, C is concentration, and γ denotes activity coefficient. As the *T* range of our experiments is above the melting point of NaCl at atmospheric pressure (801 ^{o}C), a standard state of pure liquid NaCl at *P* = 1 bar and the *T* of observation can be defined for NaCl in the silicate melt phase. For the fluid phase, a hypothetical ideal 1 molal aqueous NaCl solution at the *P* and *T* of observation can be used (Tanger and Helgeson, 1988). The ratio of $D^{fluid/melt}_{Cl}$ in the CO_2-bearing and CO_2-free systems for a given Cl concentration in the melt defines by how much the activity coefficient of the NaCl species is increased in the fluid phase by the presence of CO_2. The observation that addition of CO_2 to the system induces a drop in $D^{fluid/melt}_{Cl}$ suggests an increase of the activity coefficient of dissolved NaCl component in the aqueous fluid in response to CO_2 addition (Fig. 6). This effect can be explained by two main reasons: 1) the mean dielectric constant of the fluid decreases due to a smaller dipole moment of CO_2 compared to H_2O molecules (Holloway, 1981). 2) Na^+ and Cl^- ions as well as strongly polar associated NaCl ion pairs require the formation of hydration shells around them to be stabilized in aqueous solution. Therefore, the decreased capability of the solvent to form hydration shells is expected to increase the activity coefficients of the NaCl component in the fluid phase, consistent with the observed effect of CO_2 addition. It is likely that composition-activity relationships in the fluid phase control the variation of $D^{fluid/melt}_{Cl}$. By contract, the slight variation in H_2O concentration and the small amount of CO_2 that dissolves in the silicate melt will not have a significant effect on the structure of the melt and $D^{fluid/melt}_{Cl}$ values.

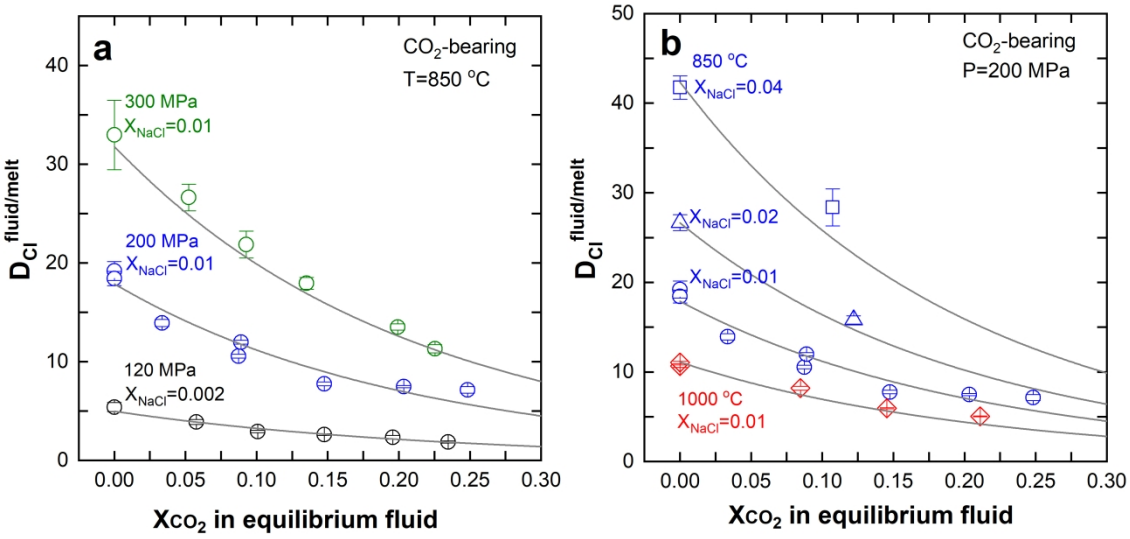

Fig. 6 Measured and calculated $D^{fluid/melt}_{Cl}$ as a function of X_{CO_2} in the fluid phase. The curves are not fits to the subset of data shown in the specific diagram but represent modeled curves using equation (6), which are essentially optimized to fit the entire dataset simultaneously **(a)** Data from 300, 200 and 120 MPa at 850 °C. Note that a constant X_{NaCl} of 0.01 was used for experiments at 300 and 200 MPa whereas at 120 MPa, a more diluted fluid (X_{NaCl}=0.002) was employed. **(b)** Data from 200 MPa at 850 and 1000 °C. $D^{fluid/melt}_{Cl}$ values increase with increasing fluid salinity (X_{NaCl} from 0.01 to 0.04) at constant *P*=200 MPa and *T*=850 °C in the presence of CO_2 by approximately the same magnitude as in the CO_2-free system. $D^{fluid/melt}_{Cl}$ decreases while *T* increases from 850 to 1000 °C at a constant X_{NaCl} of 0.01. Symbols correspond to the legend on Figure 3, except for the experiments at 850 °C and 200 MPa with X_{NaCl}=0.02 (blue triangle) and X_{NaCl}=0.04 (blue rectangle).

Our results are consistent with the limited amount of existing experimental data on systems with silicate melt compositions varying from mafic to felsic (Webster et al., 1989; Botcharnikov et al., 2007; Alletti et al., 2009; Webster et al., 2015). Alletti et al. (2009) reported that the $D^{fluid/melt}_{Cl}$ decreases approximately by a factor of 2 to 3 as CO_2 increase from 0 up to 37 mol% in the system equilibrating with basaltic melt at 100 MPa and 1200 °C at relatively dilute NaCl concentrations (X_{NaCl}=0.006-0.157; Fig. 7). Similar results were obtained for andesite melts by Botcharnikov et al.

(2007), referring that the $D^{fluid/melt}_{Cl}$ decreased by a factor of about 1.5 in response to 13-20 mol% CO_2 addition to the fluid (X_{NaCl}=0.015-0.132; Fig. 7) at 200 MPa and 1200 °C. The similarity in the extent of the effect of CO_2 on $D^{fluid/melt}_{Cl}$ in basaltic, andesitic and rhyolitic melts shows that the effect of CO_2 addition is nearly independent of the melt composition, at least at relatively dilute chloride concentrations in the fluid.

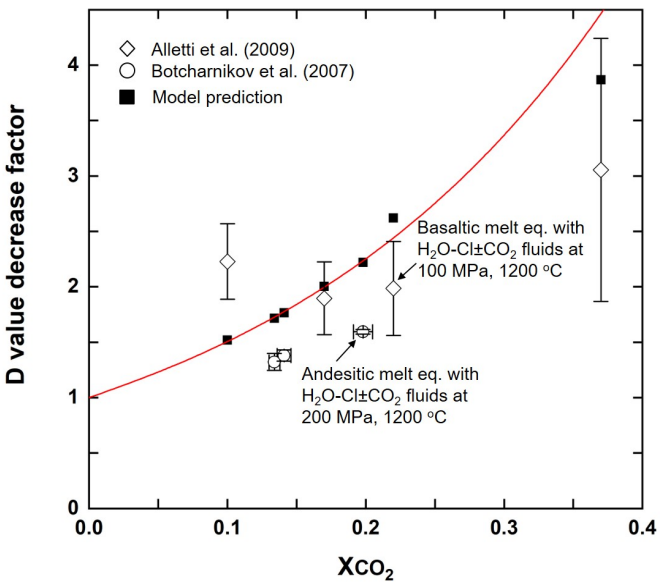

Fig. 7 The effect of CO_2 on $D^{fluid/melt}_{Cl}$ in systems with different silicate melt compositions. The filled symbols are modeled results by using Eq. (6), whereas open symbols were calculated from experimental data for basaltic melt (Alletti et al., 2009) and andesitic melt (Botcharnikov et al., 2007). Note that the deviation of the model results from following an ideal exponential curve (red line) is due to slight differences in fluid salinity (<1.5 wt%) between the CO_2-free and CO_2-bearing experiments.

In contrast, it has been shown that $D^{fluid/melt}_{Cl}$ is less affected by CO_2 addition in Cl-rich fluids in intermediate to felsic melts (Webster, 1997; Botcharnikov et al., 2007; Webster et al., 2015). Recently, Webster et al. (2015) showed that the value of $D^{fluid/melt}_{Cl}$ remains nearly constant upon

addition of ~ 10 mol% CO_2 to hydrosaline liquids equilibrated with haplogranite and phonolite melts. Since the solubility of CO_2 in hydrosaline liquids in very limited (Bowers and Helgeson, 1983), we argue, that the reason for this observation is that the added CO_2 exceeded the CO_2 solubility in the hydrosaline liquid, and as a result, most CO_2 was present as an additional CO_2-rich vapor phase in these experiments. Therefore, CO_2 addition to the system did not affect significantly the activity of NaCl in the hydrosaline-liquid phase and neither the value of $D^{fluid/melt}_{Cl}$.

However, it is notable that in our experiments the Cl concentration in the melt in the CO_2-bearing experiments appears to reach significantly higher values than in those attainable in equilibrium with CO_2-free fluids even at the highest fluid salinities. We hypothesize, that the reason for this is that the activity of NaCl component in the fluid phase(s) can achieve higher values in sub- and supercritical fluids in the presence of CO_2. Note that with the addition of the new component CO_2, the degrees of freedom in the system increase by one, which may potentially allow the variation of NaCl activity even in the vapor-liquid immiscibility field. This is also consistent with the known expansion of the solvus in response to CO_2 addition (e.g. Frantz et al., 1992; Shmulovich and Graham, 1999; Shmulovich and Graham, 2004).

4.5 An empirical model to predict $D^{fluid/melt}_{Cl}$ in granitic systems as a function of *P, T*, fluid salinity and X_{CO_2}

Based on the dataset presented above, the following empirical equation has been developed describing the variation of $\ln[D^{fluid/melt}_{Cl}]$ as a function of *P*, *T* and CO_2 and Cl concentrations in the equilibrium fluid phase:

$$\ln[D^{fluid/melt}_{Cl}] = 1.419(\pm 0.048) * \ln[P] + 0.912(\pm 0.031) * \ln\left[C^{fluid}_{Cl} + 1.434(\pm 0.260)\right] + \frac{4547(\pm 443)}{T} - 4.026(\pm 0.155) * X_{CO2} - 9.790(\pm 0.440) \quad (6)$$

where P is in MPa, T is in Kelvins, and C_{Cl}^{fluid} is the total Cl concentration in the fluid in wt%, and X_{CO_2} denotes molar fraction of CO_2 in the fluid. The major terms of the model equation reflect the observed correlation between $D_{Cl}^{fluid/melt}$ and P and fluid salinity, as well as an approximately exponential decrease of D with increasing CO_2 in the fluid. The form of temperature correction has the thermodynamic foundation of $\ln K = -\Delta_r G/RT$. All parameters were derived with a non-linear least squares regression model within the 95% confidence interval and reproduced the experimental data with 7.3% mean absolute percentage error. The predicted $D_{Cl}^{fluid/melt}$ values are shown as a function of measured values from all experiments in Figure 8. The validity of our equation is expressed by the linear regression of the logarithmic plot of Fig. 8, which results in a slope of 0.9995 (close to 1) and a Y-intercept of 0.0005 (close to 0). With X_{CO_2} approaching 1, the predicted D value converges to 0 consistent with the expected negligible solubility of NaCl in pure CO_2 gas (Zakirov et al., 2007). Furthermore, in Figure 9 the equation predicts that Cl concentration in the melt with increasing Cl in the fluid converges to a P, T, X_{CO_2} dependent value, consistent with the experimental observations. As pointed out earlier, Kravchuk and Keppler, (1994) have shown that $D_{Cl}^{fluid/melt}$ for aqueous fluid in equilibrium with near-eutectic silicate melts in the albite – quartz and albite – K-feldspar – quartz system are nearly identical to each other over a broad range of Cl concentrations (Fig. 4), and our data at 200 MPa in the CO_2-free system is identical within error to those of Webster et al. (1992a,b) obtained on K-bearing true haplogranite melts. Therefore, our model equation can be applied to evolved granitic systems with A/NK close to 1 in general, even though it was derived from a synthetic K-free system. Note that the equation is constructed in such a way that the "CO_2-term" can be applied to other systems as well, because the relative effect of CO_2 appears independent of melt composition as discussed above. However, note that we confirmed only up to X_{NaCl}=0.04 (about 12 wt% NaCl) that this relationship holds with the addition of CO_2. Using iterative calculation, the equation can be used to predict $D_{Cl}^{fluid/melt}$ at a specific Cl concentration in

the silicate melt without *a priori* knowledge of Cl concentration in the fluid. An EXCEL sheet is provided in the supplementary material for this purpose. It is important to remember that $D_{Cl}^{fluid/melt}$ becomes a meaningless quantity if liquid-vapor immiscibility occurs in the fluid phase, thus the above equation cannot be applied to systems with two-phase fluids. The reader is referred to the model of (Driesner and Heinrich, 2007) for determining the position of the solvus in the H_2O-NaCl system, but an accurate model to predict the position of the solvus in the H_2O-CO_2-NaCl system is yet to be developed.

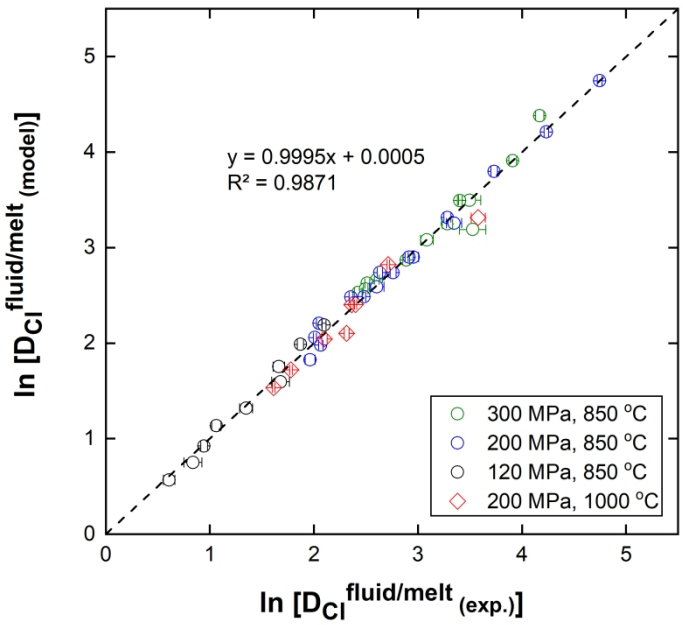

Fig. 8 Ln-ln plot of measured vs. predicted (see equation (6) in the text) $D_{Cl}^{fluid/melt}$ values from all experiments in this study. The regression line (y=0.9995*x+0.0005) indicates all data fall closely along the 1:1 line, testifying that the model accurately reproduces our experimental data.

5. Geological implications

5.1. The fate of CO_2 in arc magmas

Decreasing pressure and progressive crystallization of volatile-bearing magmas ascending through the Earth´s crust invariably leads to saturation and exsolution of a H_2O -CO_2 - Cl -rich volatile phase from the melt (e.g. Sisson and Grove, 1993; Hedenquist and Lowenstern, 1994; Wallace, 2005). If CO_2 is present in the silicate melt, fluid saturation occurs at higher pressure and temperature compared to CO_2-free systems (Dixon et al., 1995; Papale, 1999; Tamic et al., 2001). Due to the fact that the solubility of H_2O in the silicate melt increases more rapidly with increasing pressure than CO_2 solubility, it is expected that the CO_2/H_2O ratio in the exsolving fluid will increase with increasing pressure and will always be highest in the early stages of fluid exsolution. Our results highlight that if significant CO_2 is present in the melt, the coexisting fluid will not only be more CO_2-rich, but also significantly less saline at a given Cl concentration in the melt. Influx of a CO_2-rich volatile phase from an underplated mafic magma into a long-lived crustal magma reservoirs will further promote extraction of H_2O into a mixed H_2O-CO_2 bearing magmatic fluid within the upper (typically cooler and more felsic) parts of the magma reservoir. At the same time, CO_2-injection suppresses the Cl content of the exsolved volatile phase at a given melt chlorinity. Some estimates suggest that primitive arc magmas may contain as much as 1 wt% CO_2 and a typical initial water concentration of 3-4 wt% (Wallace, 2005; Blundy et al., 2010). The significantly lower CO_2 content estimated from most of the analyzed natural melt inclusions (Wallace et al., 1995; Schmitt, 2001) may result from the low probability of trapping such initial high-CO_2 melts prior to any fluid exsolution during magma ascent; therefore, arc magmas may be commonly more CO_2-rich than the 0.3% estimated, e.g., by Crisp (1984).

5.2. The effect of CO_2 on the genesis of porphyry-type ore deposit

The presence of Cl significantly enhances the solubility of many economically important metals and their transfer from silicate melt to magmatic-hydrothermal fluid by allowing the formation of

metal complexes with Cl-bearing ligands (e.g. Williams et al., 1995; e.g. Frank et al., 2002; Simon et al., 2006; Aiuppa et al., 2009; Zajacz et al., 2010; Zajacz et al., 2011). A positive relationship has been experimentally established between fluid salinity and the fluid/melt partition coefficients of several ore-forming metals and other elements (e.g. Candela and Holland, 1984; Candela and Piccoli, 1995; Bai and Koster Van Groos, 1999; Zajacz et al., 2012; Tattitch et al., 2015). Therefore, Cl-bearing fluids are believed to be essential for efficient extraction of many transition metals (e.g. notably Cu, Fe, Ag, Pb, Sn; possibly Mo, Au) enriched in porphyry type ore systems at upper crustal levels (Sillitoe, 2010). In addition, CO_2 will suppress Cl in the fluid and thereby reduce the stability of Cl-complexed metals in the aqueous-carbonic fluids, compared to CO_2-free fluids exsolved from a melt with the same Cl content. Based on the results of Kokh et al. (2017), addition of CO_2 to aqueous fluids will reduce the solubility of metals primarily dissolving in the form of electrically charged or polar metal complexes, which are normally stabilized in the fluid phase by the formation of hydration shells around them. More specifically at magmatic conditions, Tattitch et al. (2015) experimentally showed that the drop in $D^{fluid/melt}_{Cu}$ in response to CO_2 addition to the system is nearly proportional to the drop of NaCl concentration in the fluid, confirming that the fluid/melt exchange coefficient of Cu and Na are similar, independent of CO_2 concentration. Taking Na as proxy, our data therefore allow estimating the effect of CO_2 on Cu partitioning over a broader *P-T* and compositional range. Our results suggest that even small amounts of CO_2 (i.e. 5-20 mol% in the fluid, or $CO_2/H_2O \approx 0.01$ by weight in the melt) may severely limit the capability of exsolving volatiles to extract ore metals from magmas (Fig. 9). In particular, closed system degassing preventing the early escape of CO_2, or fluxing of felsic magmas with CO_2-rich fluids derived from underplated mafic magmas may inhibit effective copper extraction form the magma and thus the formation of porphyry copper deposits. Furthermore, if the magmatic fO_2 is low enough to stabilize reduced S species, it is plausible that CO_2 fluxing will increase the Au/Cu ratios in magmatic fluids as the stability of neutral and less polar Au bisulfide complexes, which are predominant at magmatic temperatures would be

less affected than those of Cu chloride complexes (Zajacz et al., 2010; Zajacz et al., 2011; Kokh et al., 2016; Kokh et al., 2017). This could be one of several factors leading to an increase of Au/Cu ratios in porphyry deposits. In addition, if chloride-rich supercritical ore fluids accumulated in felsic magma reservoirs are fluxed with CO_2, liquid (brine) saturation will be promoted due to the expansion of the vapor-liquid immiscibility field. However, as our experimental data and model calculations show, to yield high chloride concentrations in supercritical fluids or reach liquid (brine) saturation, Cl concentrations in the silicate melt will first need to achieve higher values relative to that required for effective Cl partitioning into the fluid phase in CO_2-free systems (Fig. 9). Thus, CO_2-bearing systems would have to go through more advanced crystallization building up Cl concentration in the residual melt before the onset of effective metal extraction. As a high-degree of crystallinity may impede fluid mobility and/or the attainment of equilibrium between the silicate melt and the fluid phase (Huber et al., 2012; Parmigiani et al., 2017), the ore-forming potential of shallower systems with sub-critical fluids may also be reduced by the presence of significant CO_2.

Fluid inclusions in the porphyry copper-molybdenum deposit at Butte indicate sufficient depth that fluids remain in the single-phase stability field (Rusk et al., 2004; Rusk et al., 2008). In such deep systems, the observed intermediate-density but low-salinity fluid contains at most 8 mol% of CO_2. Fluid inclusions in shallower porphyry ore deposits contain even less CO_2 prior to phase separation (Audétat et al., 2008; Landtwing et al., 2010). The generally low CO_2 content of fluids in porphyry-type Cu, Mo and Au deposits is consistent with our experimental observation that Cl and thus Cu extraction from magmas and its hydrothermal transport is optimized by low CO_2 in the mineralizing magma. Gold is also dominantly Cl-complexed at high temperatures and elevated Cl contents in magmatic fluids with low abundance of reduced S species (Stefánsson and Seward, 2003; Pokrovski et al., 2009a; Zajacz et al., 2010; Hurtig and Williams-Jones, 2015; Pokrovski et al., 2015;

Guo et al., 2018), and therefore expected to behave similarly to Cu and Na, consistent with the correlation of ore grades in many Cu-Au deposits (e.g. Ulrich and Heinrich, 2002).

5.3 The effect of CO_2 on orogenic gold deposit genesis

Mesothermal lode gold deposits contain CO_2 as a ubiquitous major component in fluid inclusions (Robert and Kelly, 1987; Diamond and Marshall, 1990; Groves et al., 1998; Goldfarb et al., 2001; Goldfarb and Groves, 2015). According to some authors, these are also related to mid-crustal magmatic intrusions (Cameron and Hattori, 1987; Spooner, 1993; Sillitoe and Thompson, 1998; Graupner et al., 2006; Mueller et al., 2008; Doublier et al., 2014). Muruntau (Uzbekistan) is a giant mesothermal gold-bearing quartz vein deposit above a large granite intrusion, formed by low- to intermediate NaCl fluids containing up to 15 mol% CO_2 with lower amounts of N_2 and CH_4 in early, high-*T* fluid inclusions (Graupner et al., 2001). So-called intrusion-related gold deposits have ore fluid compositions that are essentially identical to those of typical orogenic lode gold deposits, with low salinity (3-10 wt% NaCl equiv) but at least 5 mol% CO_2 (Thompson et al., 1999). CO_2-rich fluids are expected to exsolve in an ascending pluton as the first-saturating volatile phase, initially extracting the greatest fraction of available CO_2, along with other highly volatile components, notably H_2S (Cameron and Hattori, 1987). Carbon dioxide suppresses the extraction of not only Cl but also Cl-complexed base metals from such deep magmas. On the other hand, the expected high concentration of H_2S will selectively favor the extraction of sulfide-complexed metals, notably Au, because gold forms its most stable complexes with reduced sulfur ligands (e.g. $Au(HS)^0$,$Au(HS)_2^-$, $NaAu(HS)_2$ and $Au(HS)S_3^-$ (Stefánsson and Seward, 2004; Simon et al., 2007; Pokrovski et al., 2009b; Zajacz et al., 2010; Pokrovski et al., 2015). At magmatic *T*, uncharged species are expected to be most stable, so that CO_2 would not significantly reduce gold solubility (Kokh et al., 2016; Kokh et al., 2017). Therefore, along with the conclusions of the above studies on metal complex stabilities,

our experimental data imply that CO_2-rich fluids exsolved from magmas at an earlier stage of evolution and/or at greater depths favor the formation of base-metal poor but gold-rich vein deposits, as observed in many orogenic gold provinces involving late granitoid intrusions.

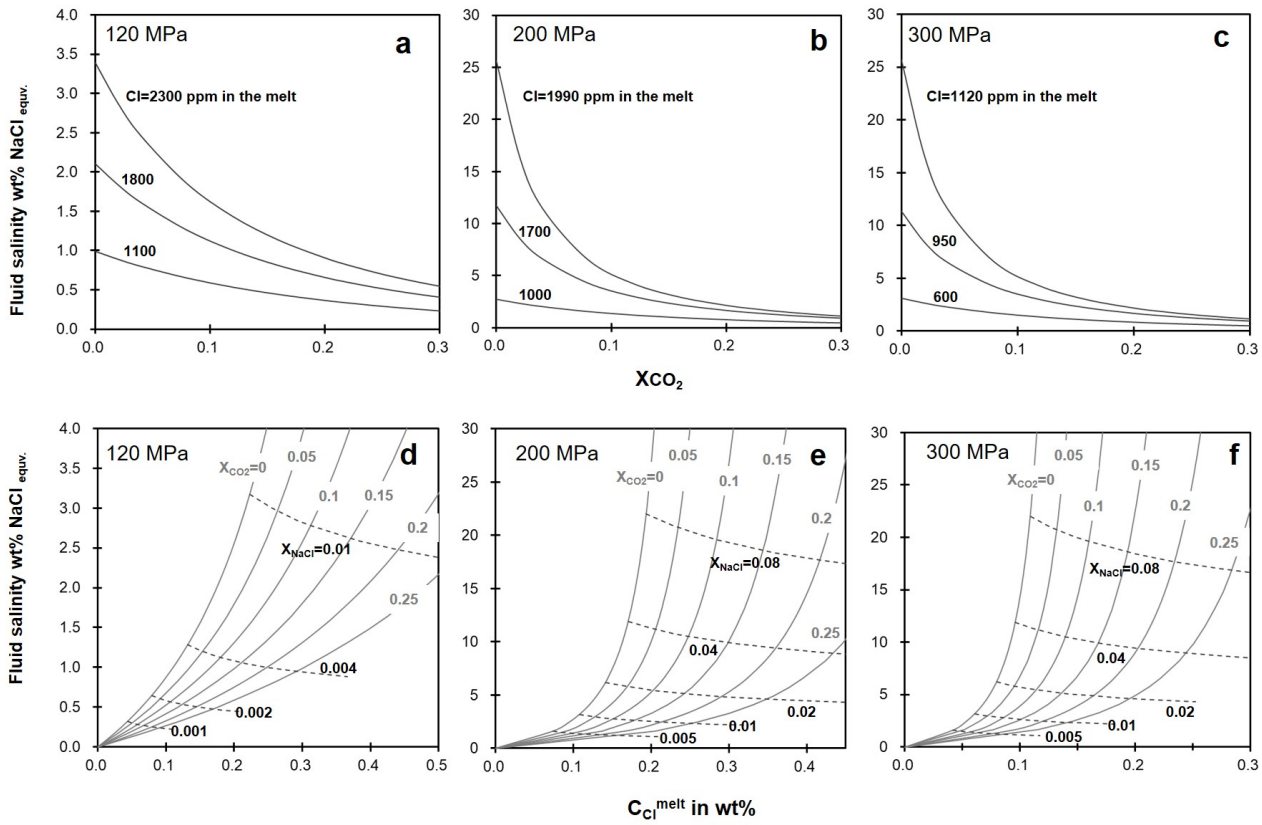

Fig 9. Predicted chloride concentrations in fluids in equilibrium with slightly peraluminous haplogranitic melts as a function of Cl concentration in the melt and CO_2 concentration in the fluid phase. Contour lines on plots **a, b** and **c** show the predicted NaCl concentration in the fluid as a function of X_{CO_2} in the fluid for different Cl concentrations in the melt (labels next to curves) at 120, 200 and 300 MPa confining pressure. Note that the relative effect of CO_2 at a constant Cl concentration in the melt is even stronger than at a constant Cl concentration in the fluid. Plots **d, e** and **f** display the predicted NaCl concentrations in the fluid phase as a function of Cl concentration in the melt at various X_{CO2} in the fluid (label next to the curves). Results are modeled at T=850 °C.

6. Conclusions

The addition of CO_2 into aqueous metal chloride-bearing fluids results in a decrease of $D^{fluid/melt}_{Cl}$ in the granitoid melt at *P-T* conditions of 120 – 300 MPa and 850 – 1000 °C. The value of $D^{fluid/melt}_{Cl}$ decreases by a factor of about 2-3 in response to the addition of 20-25 mol% of CO_2 to the fluid. The relative effect of CO_2 addition appears independent of *P*, *T*, and fluid salinity, at least up to about 12 wt% NaCl equivalent salt concentration. An empirical equation is presented that can be utilized to calculate $D^{fluid/melt}_{Cl}$ as a function of *P, T*, Cl and CO_2 concentration in the fluid for metaluminous to slightly peraluminous granitic melt compositions, that are most common at convergent plate boundaries. This equation can be employed to quantitatively model chloride concentrations in aqueous-carbonic fluids released from ascending magmas and/or crystallizing felsic plutons. As chlorine is an important ligand for the dissolution of several ore metals in magmatic fluids (e.g. Cu, Ag, Pb, Zn, Sn), CO_2 addition will suppress the extraction of these metals from magmas by exsolving fluids. This is consistent with the observation that high-T fluids in most economic porphyry-copper and related base-metal vein deposits are CO_2-poor. More deeply formed mesothermal vein deposits are base-metal poor but gold-rich, possibly because Au extraction from deeper magmas is promoted by early exsolution of CO_2-H_2S-SO_2-rich fluids with low salinity, consistent with fluid inclusion observations.

Acknowledgements

This work was supported by the ETH research grant ETH-21 12-2. We gratefully thank Denis Zezin for his assistance and discussions on programming the fitting model. We would also like to thank for constructive comments by Michael Carroll, Michel Pichavant, Brian Tattitch and an anonymous reviewer, which helped us to improve the quality of the manuscript, and we are grateful to Gleb Pokrovski for his editorial handling of the manuscript. Z. Zajacz would like to acknowledge the Swiss National Science Foundation (Ambizione grant no. PZ00P2_136857) and the Natural

Sciences and Engineering Research Council of Canada – Discovery Grant Program for financial support.

References

Aiuppa A., Baker D. R. and Webster J. D. (2009) Halogens in volcanic systems. *Chem. Geol.* **263**, 1– 18.

Alletti M., Baker D. R., Scaillet B., Aiuppa A., Moretti R. and Ottolini L. (2009) Chlorine partitioning between a basaltic melt and H_2O-CO_2 fluids at Mount Etna. *Chem. Geol.* **263**, 37–50. Available at: http://dx.doi.org/10.1016/j.chemgeo.2009.04.003.

Anderko A. and Pitzer K. S. (1993) Equation-of-state representation of phase equilibria and volumetric properties of the system NaCl-H_2O above 573 K. *Geochim. Cosmochim. Acta* **57**, 1657–1680.

Audétat A., Pettke T., Heinrich C. A., Bodnar R. J., Audétat A., Pettke T., Heinrich C. A. and Bodnar R. J. (2008) The composition of magmatic-hydrothermal fluids in barren and mineralized intrusions. *Econ. Geol.* **103**, 877–908.

Bai T. B. and Koster Van Groos A. F. (1999) The distribution of Na, K, Rb, Sr, Al, Ge, Cu, W, Mo, La, and Ce between granitic melts and coexisting aqueous fluids. *Geochim. Cosmochim. Acta* **63**, 1117–1131.

Beermann O., Botcharnikov R. E. and Nowak M. (2015) Partitioning of sulfur and chlorine between aqueous fluid and basaltic melt at 1050°C, 100 and 200 MPa. *Chem. Geol.* **418**, 132–157. Available at: http://dx.doi.org/10.1016/j.chemgeo.2015.08.008.

Behrens H., Ohlhorst S., Holtz F. and Champenois M. (2004) CO_2 solubility in dacitic melts equilibrated with H_2O-CO_2 fluids: Implications for modeling the solubility of CO2 in silicic melts. *Geochim. Cosmochim. Acta* **68**, 4687–4703.

Blundy J., Cashman K. V., Rust A. and Witham F. (2010) A case for CO_2-rich arc magmas. *Earth Planet. Sci. Lett.* **290**, 289–301. Available at: http://dx.doi.org/10.1016/j.epsl.2009.12.013.

Bodnar R. J., Burnham C. W. and Sterner S. M. (1985) Synthetic fluid inclusions in natural quartz. III. Determination of phase equilibrium properties in the system H_2O-NaCl to 1000°C and 1500 bars. *Geochim. Cosmochim. Acta* **49**, 1861–1873.

Botcharnikov R. E., Behrens H., Holtz F., Koepke J. and Sato H. (2004) Sulfur and chlorine solubility in Mt. Unzen rhyodacitic melt at 850 °C and 200 MPa. *Chem. Geol.* **213**, 207–225.

Botcharnikov R. E., Holtz F. and Behrens H. (2015) Solubility and fluid-melt partitioning of H_2O and Cl in andesitic magmas as a function of pressure between 50 and 500 MPa. *Chem. Geol.* **418**, 117–131. Available at: http://dx.doi.org/10.1016/j.chemgeo.2015.07.019.

Botcharnikov R. E., Holtz F. and Behrens H. (2007) The effect of CO_2 on the solubility of H_2O-Cl fluids in andesitic melt. *Eur. J. Miner.* **19**, 671–680.

Bowers T. S. and Helgeson H. C. (1983) Calculation of the thermodynamic and geochemical consequences of nonideal mixing in the system H_2O-CO_2-NaCl on phase relations in geologic systems: metamorphic equilibria at high pressures and temperatures. *Geochim. Cosmochim. Acta* **47**, 1247–1275.

Cameron E. M. and Hattori K. (1987) Archean gold mineralization and oxidized hydrothermal fluids. *Econ. Geol.* **82**, 1177–1191.

Candela P. A. and Holland H. D. (1984) The partitioning of copper and molybdenum between silicate melts and aqueous fluids. *Geochim. Cosmochim. Acta* **48**, 373–380.

Candela P. A. and Piccoli P. M. (1995) Model ore metal partitioning from melts into vapor and vapor/ brine mixtures. In *Magmas, fluids, and ore deposits* (ed. J. F. H. Thompson). University of British Columbia. pp. 101–127.

Chou I.-M. (1987) Oxygen buffer and hydrogen sensor techniques at elevated pressures and temperatures. In *Hydrothermal Experimental Techniques* (eds. G. C. ULMER and H. L. BARNES). Wiley-Interscience, New York.

Chou I.-M. and Eugster H. P. (1977) Solubility of magnetite in supercritical chloride solutions. *Am. J. Sci.* **277**, 1296–1314.

Crerar D. A. and Barnes H. L. (1976) Ore solution chemistry. V. Solubilities of chalcopyrite and chalcocite assemblages in hydrothermal solutions at 200 to 350 ^{o}C. *Econ. Geol.* **71**, 772–794.

Crisp J. A. (1984) Rates of magma emplacement and volcanic output. *J. Volcanol. Geotherm. Res.* **20**, 177–211.

Diamond L. W. and Marshall D. D. (1990) Evaluation of the fluid-inclusion crushing-stage as an aid in exploration for mesothermal gold-quartz deposits. *J. Geochemical Explor.* **38**, 285–297.

Dixon J. E., Stolper E. M. and Holloway J. R. (1995) An Experimental Study of Water and Carbon Dioxide Solubilities in Mid-Ocean Ridge Basaltic Liquids. Part I: Calibration and solubility models. *J. Petrol.* **36**, 1607–1631. Available at: https://academic.oup.com/petrology/article/36/6/1633/1493324/An-Experimental-Study-of-Water-and-Carbon-Dioxide.

Dolejš D. and Zajacz Z. (2018) Halogens in Silicic Magmas and Their Hydrothermal Systems. In *The Role of Halogens in Terrestrial and Extraterrestrial Geochemical Processes* (eds. D. E. Harlov and L. Aranovich). Springer, Cham. pp. 431–543.

Doublier M. P., Thébaud N., Wingate M. T. D., Romano S. S., Kirkland C. L., Gessner K., Mole D. R. and Evans N. (2014) Structure and timing of Neoarchean gold mineralization in the Southern Cross district (Yilgarn Craton, Western Australia) suggest leading role of late Low-Ca I-type

granite intrusions. *J. Struct. Geol.* **67**, 205–221.

Driesner T. (2007) The system H_2O-NaCl. Part II: Correlations for molar volume, enthalpy, and isobaric heat capacity from 0 to 1000 °C, 1 to 5000 bar, and 0 to 1 XNaCl. *Geochim. Cosmochim. Acta* **71**, 4902–4919.

Driesner T. and Heinrich C. A. (2007) The system H_2O-NaCl. Part I: Correlation formulae for phase relations in temperature-pressure-composition space from 0 to 1000 °C, 0 to 5000 bar, and 0 to 1 XNaCl. *Geochim. Cosmochim. Acta* **71**, 4880–4901.

Driesner T., Seward T. M. and Tironi I. G. (1998) Molecular dynamics simulation study of ionic hydration and ion association in dilute and 1 molal aqueous sodium chloride solutions from ambient to supercritical conditions. *Geochim. Cosmochim. Acta* **62**, 3095–3107.

Duan Z., Moller N. and Weare J. W. (1995) Equation of state for the NaCl-H_2O-CO_2 system; prediction of phase equilibria and volumetric properties. *Geochim. Cosmochim. Acta* **59**, 2869–2882.

Frank M. R., Candela P. A., Piccoli P. M. and Glascock M. D. (2002) Gold solubility, speciation, and partitioning as a function of HCl in the brine-silicate melt-metallic gold system at 800°C and 100 MPa. *Geochim. Cosmochim. Acta* **66**, 3719–3732.

Frank M. R., Simon A. C., Pettke T., Candela P. A. and Piccoli P. M. (2011) Gold and copper partitioning in magmatic-hydrothermal systems at 800°C and 100MPa. *Geochim. Cosmochim. Acta* **75**, 2470–2482. Available at: http://dx.doi.org/10.1016/j.gca.2011.02.012.

Frantz J. D., Popp R. K. and Hoering T. C. (1992) The compositional limits of fluid immiscibility in the system H_2O-NaCl-CO_2 as determined with the use of synthetic fluid inclusions in conjunction with mass spectrometry. *Chem. Geol.* **98**, 237–255.

Goldfarb R. J. and Groves D. I. (2015) Orogenic gold: Common or evolving fluid and metal sources through time. *Lithos* **233**, 2–26. Available at: http://dx.doi.org/10.1016/j.lithos.2015.07.011.

Goldfarb R. J. J., Groves D. I. I. and Gardoll S. (2001) Orogenic gold and geologic time: A global synthesis. *Ore Geol. Rev.* **18**, 1–75.

Graupner T., Kempe U., Spooner E. T. C., Bray C. J., Krementenetsky A. A. and Irmer G. (2001) Microthermometric, laser raman spectroscopic, and volatile-on chromatographic analysis of hydrothermal fluids in the paleozoic Muruntau Au-bearing quartz vein ore field, Uzbekistan. *Econ. Geol.* **96**, 1–23.

Graupner T., Niedermann S., Kempe U., Klemd R. and Bechtel A. (2006) Origin of ore fluids in the Muruntau gold system: Constraints from noble gas, carbon isotope and halogen data. *Geochim. Cosmochim. Acta* **70**, 5356–5370.

Grove T. L., Elkins-Tanton L. T., Parman S. W., Chatterjee N., Müntener O. and Gaetani G. A. (2003) Fractional crystallization and mantle-melting controls on calc-alkaline differentiation trends. *Contrib. to Mineral. Petrol.* **145**, 515–533.

Groves D. I., Goldfarb R. J., Gebre-Mariam M., Hagemann S. G. and Robert F. (1998) Orogenic gold deposits: A proposed calssification in the context of their crustal contribution and relationship to other gold deposit types. *Ore Geol. Rev.* **13**, 7–27.

Guo H., Audétat A. and Dolejš D. (2018) Solubility of gold in oxidized, sulfur-bearing fluids at 500–850 °C and 200–230 MPa: A synthetic fluid inclusion study. *Geochim. Cosmochim. Acta* **222**, 655–670.

Hedenquist J. W. and Lowenstern J. B. (1994) The role of magmas in the formation of hydrothermal ore deposits. *Nature* **370**, 519–527.

Helgeson H. C. (1981) Prediction of the thermodynamic properties of electrolytes at high pressures and temperatures. *Phys. Chem. Earth* **13–14**, 133–177.

Helgeson H. C. (1969) Thermodynamics of hydrothermal systems at elevated temperatures and pressures. *Am. J. Sci.* **267**, 729–804.

Holland H. D. (1972) Granites, solutions, and base metal deposits. *Econ. Geol.* **67**, 281–301.

Holloway J. R. (1981) Compositions and volumes of supercritical fluids in earth's crust. In *Short Course in Fluid Inclusions:Application to Petrology* (ed. M. L. Hollister, L. S., Crawford). pp. 13–35.

Huber C., Bachmann O., Vigneresse J. L., Dufek J. and Parmigiani A. (2012) A physical model for metal extraction and transport in shallow magmatic systems. *Geochemistry, Geophys. Geosystems* **13**, 1–18.

Hurtig N. C. and Williams-Jones A. E. (2015) Porphyry-epithermal Au-Ag-Mo ore formation by vapor-like fluids: New insights from geochemical modeling. *Geology* **43**, 587–590.

Joyce D. B. and Holloway J. R. (1993) An experimental determination of the thermodynamic properties of H_2O-CO_2-NaCl fluids at high pressures and temperatures. *Geochim. Cosmochim. Acta* **57**, 733–746.

Kokh M. A., Akinfiev N. N., Pokrovski G. S., Salvi S. and Guillaume D. (2017) The role of carbon dioxide in the transport and fractionation of metals by geological fluids. *Geochim. Cosmochim. Acta* **197**, 433–466. Available at: http://dx.doi.org/10.1016/j.gca.2016.11.007.

Kokh M. A., Lopez M., Gisquet P., Lanzanova A., Candaudap F., Besson P. and Pokrovski G. S. (2016) Combined effect of carbon dioxide and sulfur on vapor-liquid partitioning of metals in hydrothermal systems. *Geochim. Cosmochim. Acta* **187**, 311–333.

Kravchuk I. F. and Keppler H. (1994) Distribution of chloride between aqueous fluids and felsic melts at 2 kbar and 800oC. *Eur. J. Miner.* **6**, 913–923.

Landtwing M. R., Furrer C., Redmond P. B., Pettke T., Guillong M. and Heinrich C. A. (2010) The Bingham Canyon porphyry Cu-Mo-Au deposit. III. Zoned copper-gold ore deposition by magmatic vapor expansion. *Econ. Geol.* **105**, 91–118.

Mathez E. A. and Webster J. D. (2005) Partitioning behavior of chlorine and fluorine in the system apatite-silicate melt-fluid. *Geochim. Cosmochim. Acta* **69**, 1275–1286.

Mei Y., Liu W., Sherman D. M. and Brugger J. (2014) Metal complexation and ion hydration in low density hydrothermal fluids: Ab initio molecular dynamics simulation of Cu(I) and Au(I) in chloride solutions (25-1000°C, 1-5000bar). *Geochim. Cosmochim. Acta* **131**, 196–212.

Metrich N. and Rutherford M. J. (1992) Experimental study of chlorine behavior in hydrous silicic melts. *Geochim. Cosmochim. Acta* **56**, 607–616.

Mueller A. G., Hall G. C., Nemchin A. A., Stein H. J., Creaser R. A. and Mason D. R. (2008) Archean high-Mg monzodiorite-syenite, epidote skarn, and biotite-sericite gold lodes in the Granny Smith-Wallaby district, Australia: U-Pb and Re-Os chronometry of two intrusion-related hydrothermal systems. *Miner. Depos.* **43**, 337–362.

Nandedkar R. H., Ulmer P. and Müntener O. (2014) Fractional crystallization of primitive, hydrous arc magmas: An experimental study at 0.7 GPa. *Contrib. to Mineral. Petrol.* **167**, 1–27.

Papale P. (1999) Modeling of the solubility of two-component H2O + CO2 fluid in silicate liquids. *Am. Mineral.* **84**, 477–492. Available at: http://link.springer.com/article/10.1007%2Fs004100050247.

Papale P., Moretti R. and Barbato D. (2006) The compositional dependence of the saturation surface of H_2O + CO_2 fluids in silicate melts. *Chem. Geol.* **229**, 78–95.

Parmigiani A., Degruyter W., Leclaire S., Huber C. and Bachmann O. (2017) The mechanics of shallow magma reservoir outgassing. *Geochemistry, Geophys. Geosystems* **18**, 2887–2905.

Pokrovski G. S., Kokh M. A., Guillaume D., Borisova A. Y., Gisquet P., Hazemann J.-L., Lahera E., Del Net W., Proux O., Testemale D., Haigis V., Jonchière R., Seitsonen A. P., Ferlat G., Vuilleumier R., Saitta A. M., Boiron M.-C. and Dubessy J. (2015) Sulfur radical species form gold deposits on Earth. *Proc. Natl. Acad. Sci.* **112**, 13484–13489. Available at: http://www.pnas.org/lookup/doi/10.1073/pnas.1506378112.

Pokrovski G. S., Tagirov B. R., Schott J., Bazarkina E. F., Hazemann J. L. and Proux O. (2009a) An in situ X-ray absorption spectroscopy study of gold-chloride complexing in hydrothermal fluids. *Chem. Geol.* **259**, 17–29.

Pokrovski G. S., Tagirov B. R., Schott J., Hazemann J. L. and Proux O. (2009b) A new view on gold speciation in sulfur-bearing hydrothermal fluids from in situ X-ray absorption spectroscopy and quantum-chemical modeling. *Geochim. Cosmochim. Acta* **73**, 5406–5427.

Robert F. and Kelly W. C. (1987) Ore-Forming Fluids in Archean Gold-Bearing Quartz Veins At the Sigma-Mine, Abitibi Greenstone-Belt, Quebec, Canada. *Econ. Geol.* **82**, 1464–1482.

Rusk B. G., Reed M. H. and Dilles J. H. (2008) Fluid inclusion evidence for magmatic-hydrothermal fluid evolution in the porphyry copper-molybdenum deposit at Butte, Montana. *Econ. Geol.* **103**, 307–334.

Rusk B. G., Reed M. H., Dilles J. H., Klemm L. M. and Heinrich C. A. (2004) Compositions of magmatic hydrothermal fluids determined by LA-ICP-MS of fluid inclusions from the porphyry copper-molybdenum deposit at Butte, MT. *Chem. Geol.* **210**, 173–190.

Schmitt A. K. (2001) Gas-saturated crystallization and degassing in large-volume, crystal-rich dacitic magmas from the Altiplano-Puna, northern Chile. *J. Geophys. Res. Solid Earth* **106**, 30561–30578.

Seward T. M. (1981) Metal complex formation in aqueous solutions at elevated temperatures and pressures. *Phys. Chem. Earth* **13–14**, 113–132.

Shinohara H. (2009) A missing link between volcanic degassing and experimental studies on chloride partitioning. *Chem. Geol.* **263**, 51–59. Available at: http://dx.doi.org/10.1016/j.chemgeo.2008.12.001.

Shinohara H. (1994) Exsolution of immiscible vapor and liquid phases from a crystallizing silicate melt: Implications for chlorine and metal transport. *Geochim. Cosmochim. Acta* **58**, 5215–5221.

Shinohara H., Iiyama J. T. and Matsuo S. (1989) Partition of chlorine compounds between silicate melt and hydrothermal solutions: I. Partition of NaCl-KCl. *Geochim. Cosmochim. Acta* **53**, 2617–2630.

Shishkina T. A., Botcharnikov R. E., Holtz F., Almeev R. R. and Portnyagin M. V. (2010) Solubility of H_2O- and CO_2-bearing fluids in tholeiitic basalts at pressures up to 500MPa. *Chem. Geol.* **277**, 115–125. Available at: http://dx.doi.org/10.1016/j.chemgeo.2010.07.014.

Shmulovich K. I. and Graham C. M. (1999) An experimental study of phase equilibria in the system H_2O-CO_2 -NaCl at 800 ° C and 9 kbar. *Contrib. to Mineral. Petrol.* **136**, 247–257. Available at: http://www.scopus.com/inward/record.url?eid=2-s2.0-0033429550&partnerID=40&md5=eb1fbf1dbc97c0db7811fe094514dcd6.

Shmulovich K. I. and Graham C. M. (2004) An experimental study of phase equilibria in the systems H_2O-CO_2-$CaCl_2$ and H_2O-CO_2-NaCl at high pressures and temperatures (500-800 oC, 0.5-0.9

GPa): Geological and geophysical applications. *Contrib. to Mineral. Petrol.* **146**, 450–462.

Signorelli S. and Carroll M. R. (2002) Experimental study of Cl solubility in hydrous alkaline melts: Constraints on the theoretical maximum amount of Cl in trachytic and phonolitic melts. *Contrib. to Mineral. Petrol.* **143**, 209–218.

Signorelli S. and Carroll M. R. (2000) Solubility and fluid-melt partitioning of Cl in hydrous phonolitic melts. *Geochim. Cosmochim. Acta* **64**, 2851–2862.

Sillitoe R. H. (2010) Porphyry copper systems. *Econ. Geol.* **105**, 3–41.

Sillitoe R. H. and Thompson J. F. H. (1998) Intrusion-Related Vein Gold Deposits: Types, Tectono-Magmatic Settings and Difficulties of Distinction from Orogenic Gold Deposits. *Resour. Geol.* **48**, 237–250.

Simon A. C., Pettke T., Candela P. A., Piccoli P. M. and Heinrich C. A. (2006) Copper partitioning in a melt-vapor-brine-magnetite-pyrrhotite assemblage. *Geochim. Cosmochim. Acta* **70**, 5583–5600.

Simon A. C., Pettke T., Candela P. A., Piccoli P. M. and Heinrich C. A. (2007) The partitioning behavior of As and Au in S-free and S-bearing magmatic assemblages. *Geochim. Cosmochim. Acta* **71**, 1764–1782.

Sisson T. W. and Grove T. L. (1993) Experimental investigations of the role of H_2O in calc-alkaline differentiation and subduction zone magmatism. *Contrib. to Mineral. Petrol.* **113**, 143–166.

Spooner E. T. C. (1993) Magmatic sulphide/volatile interaction as a mechanism for producing chalcophile element enriched, Archean Au-quartz, epithermal AuAg and Au skarn hydrothermal ore fluids. *Ore Geol. Rev.* **7**, 359–379.

Stefánsson A. and Seward T. M. (2004) Gold(I) complexing in aqueous sulphide solutions to 500°C at 500 bar. *Geochim. Cosmochim. Acta* **68**, 4121–4143.

Stefánsson A. and Seward T. M. (2003) Stability of chloridogold(I) complexes in aqueous solutions from 300 to 600°C and from 500 to 1800 bar. *Geochim. Cosmochim. Acta* **67**, 4559–4576.

Stelling J., Botcharnikov R. E., Beermann O. and Nowak M. (2008) Solubility of H_2O- and chlorine-bearing fluids in basaltic melt of Mount Etna at T = 1050-1250 °C and P = 200 MPa. *Chem. Geol.* **256**, 101–109. Available at: http://dx.doi.org/10.1016/j.chemgeo.2008.04.009.

Tamic N., Behrens H. and Holtz F. (2001) The solubility of H_2O and CO_2 in rhyolitic melts in equilibrium with a mixed CO_2-H_2O fluid phase. *Chem. Geol.* **174**, 333–347.

Tanger J. C. and Helgeson H. C. (1988) Calculation of the thermodynamic and transport properties of aqueous species at high pressures and temperatures; revised equations of state for the standard partial molal properties of ions and electrolytes. *Am. J. Sci.* **288**, 19–98.

Tattitch B. C., Candela P. A., Piccoli P. M. and Bodnar R. J. (2015) Copper partitioning between felsic melt and H_2O-CO_2 bearing saline fluids. *Geochim. Cosmochim. Acta* **148**, 81–99. Available at: http://dx.doi.org/10.1016/j.gca.2014.08.025.

Thompson J. F. H. H., Sillitoe R. H., Baker T., Lang J. R. and Mortensen J. K. (1999) Intrusion-related gold deposits associated with tungsten-tin provinces. *Miner. Depos.* **34**, 323–334.

Ulmer P., Kaegi R. and Müntener O. (2018) Experimentally derived intermediate to silica-rich arc magmas by fractional and equilibrium crystallization at 1·0 GPa: An evaluation of phase relationships, compositions, liquid lines of descent and oxygen fugacity. *J. Petrol.* **59**, 11–58.

Ulrich T. and Heinrich C. A. (2002) Geology and alteration geochemistry of the porphyry Cu-Au deposit at Bajo de la Alumbrera, Argentina. *Econ. Geol.* **97**, 1865–1886.

Wallace P. J. (2005) Volatiles in subduction zone magmas: Concentrations and fluxes based on melt inclusion and volcanic gas data. *J. Volcanol. Geotherm. Res.* **140**, 217–240.

Wallace P. J., Anderson A. T. and Davis A. M. (1995) Quantification of pre-eruptive exsolved gas contents in silicic magmas. *Nature* **377**, 612–616.

Webster J. D. (1997) Exsolution of magmatic volatile phases from Cl-enriched mineralizing granitic magmas and implications for ore metal transport. *Geochim. Cosmochim. Acta* **61**, 1017–1029.

Webster J. D. (1992a) Fluid-melt interactions involving Cl-rich granites. Experimental study from 2 to 8 Kb. *Geochim. Cosmochim. Acta* **56**, 659–678.

Webster J. D. (1992b) Water solubility and chlorine partitioning in Cl-rich granitic systems: Effects of melt composition at 2 kbar and 800°C. *Geochim. Cosmochim. Acta* **56**, 679–687.

Webster J. D., Goldoff B., Sintoni M. F., Shimizu N. and De Vivo B. (2014) C-O-H-Cl-S-F volatile solubilities, partitioning, and mixing in phonolitic-trachytic melts and aqueous-carbonic vapor ± saline liquid at 200MPa. *J. Petrol.* **55**, 2217–2248.

Webster J. D. and Holloway J. R. (1988) Experimental constraints on the partitioning of Cl between topaz rhyolite melt and H2O and H2O+CO2 fluids: New implications for granitic differentiation and ore deposition. *Geochim. Cosmochim. Acta* **52**, 2091–2105.

Webster J. D., Holloway J. R. and Hervig R. L. (1989) Partitioning of lithophile trace elements between H2O and H2O + CO2 fluids and topaz rhyolite melt. *Econ. Geol.* **84**, 116–134.

Webster J. D., Kinzler R. J. and Mathez E. A. (1999) Chloride and water solubility in basalt and andesite melts and implications for magmatic degassing. *Geochim. Cosmochim. Acta* **63**, 729–738.

Webster J. D., Sintoni M. F. and De Vivo B. (2009) The partitioning behavior of Cl, S, and H_2O in aqueous vapor- ± saline-liquid saturated phonolitic and trachytic melts at 200 MPa. *Chem. Geol.*

263, 19–36. Available at: http://dx.doi.org/10.1016/j.chemgeo.2008.10.017.

Webster J. D., Vetere F., Botcharnikov R. E., Goldoff B., McBirney A. and Doherty A. L. (2015) Experimental and modeled chlorine solubilities in aluminosilicate melts at 1 to 7000 bars and 700 to 1250 °c: Applications to magmas of Augustine Volcano, Alaska. *Am. Mineral.* **100**, 522–535.

Webster J. D. and De Vivo B. (2002) Experimental and modeled solubilities of chlorine in aluminosilicate melts, consequences of magma evolution, and implications for exsolution of hydrous chloride melt at Mt. Somma-Vesuvius. *Am. Mineral.* **87**, 1046–1061.

Williams-Jones A. E. and Heinrich C. A. (2005) 100th Anniversary Special Paper: Vapor transport of metals and the formation of magmatic-hydrothermal ore deposits. *Econ. Geol.* **100**, 1287–1312.

Williams T. J., Candela P. A. and Piccoli P. M. (1997) Hydrogen-alkali exchange between silicate melts and two-phase aqueous mixtures: an experimental investigation. *Contrib. to Mineral. Petrol.* **128**, 114–126.

Williams T. J., Candela P. A. and Piccoli P. M. (1995) The partitioning of copper between silicate melts and two-phase aqueous fluids: An experimental investigation at 1 kbar, 800° C and 0.5 kbar, 850° C. *Contrib. to Mineral. Petrol.* **121**, 388–399.

Zajacz Z., Candela P. A., Piccoli P. M. and Sanchez-Valle C. (2012) The partitioning of sulfur and chlorine between andesite melts and magmatic volatiles and the exchange coefficients of major cations. *Geochim. Cosmochim. Acta* **89**, 81–101.

Zajacz Z., Halter W. E., Pettke T. and Guillong M. (2008) Determination of fluid/melt partition coefficients by LA-ICPMS analysis of co-existing fluid and silicate melt inclusions: Controls on element partitioning. *Geochim. Cosmochim. Acta* **72**, 2169–2197.

Zajacz Z., Seo J. H., Candela P. A., Piccoli P. M., Heinrich C. A. and Guillong M. (2010) Alkali metals control the release of gold from volatile-rich magmas. *Earth Planet. Sci. Lett.* **297**, 50–56. Available at: http://dx.doi.org/10.1016/j.epsl.2010.06.002.

Zajacz Z., Seo J. H., Candela P. A., Piccoli P. M. and Tossell J. A. (2011) The solubility of copper in high-temperature magmatic vapors: A quest for the significance of various chloride and sulfide complexes. *Geochim. Cosmochim. Acta* **75**, 2811–2827.

Zakirov I. V., Sretenskaja N. G., Aranovich L. Y. and Volchenkova V. A. (2007) Solubility of NaCl in CO_2 at high pressure and temperature: First experimental measurements. *Geochim. Cosmochim. Acta* **71**, 4251–4255.

Table 1. The composition of the starting glasses

	GL6 (anh.)	HGL6-1 (hyd.)*	HGL6-3 (hyd.)*	HGL6-5 (hyd.)*
n	106	20	60	50
SiO_2	80.1 (0.7)	78.4 (1.7)	79.8 (0.8)	79.7 (1.3)
Al_2O_3	12.6 (0.2)	13.7 (0.7)	12.9 (0.3)	13.0 (0.5)
Na_2O	7.3 (0.3)	7.9 (0.4)	7.3 (0.3)	7.3 (0.3)
K_2O	0.02 (0.01)	0.02 (0.01)	0.02 (0.01)	0.02 (0.01)
Total	99.6 (0.8)	93.4 (1.0)	94.5 (0.8)	93.4 (1.2)
molar A/NK	1.039 (0.039)	1.051 (0.029)	1.064 (0.045)	1.084 (0.025)

anh.: anhydrous composition, hyd.:hydrous composition, n : number of analyses averaged
molar A/NK: molar Al_2O_3/Na_2O+K_2O ratio in the starting glasses
* Hydrous glasses synthesized at 200 MPa, 1050 °C with 5 wt% H_2O added.
Note that we report concentrations in wt% normalized to yield a total of 100 to allow easy comparison of the anhydrous and hydrous glasses. Nevertheless, the original analysis totals are shown to demonstrate the quality of analysis. The measured uncertainties (1 σ) are shown in parenthesis.

Table 2. Experimental run conditions and Cl concentrations in the aqueous fluid and melt for the CO_2-free system

Run no.	P (MPa)	Run duration (h)	Starting glass	Glass (mg)	Solution (mg)	Total mCl[a]	X_{NaCl}[b]	Cl in melt (ppm)	Wt% H_2O in melt[c]	A/NK[d]	HCl/NaCl in fluid[e]	$D_{Cl}^{fluid/melt}$	$D_{Cl}^{fluid/melt}$ (modeled)[f]
Experiments conducted at T=850 °C													
#10c	299 ± 1	48	GL6	8.08	7.87	0.292	0.0050	315 (40)	7.3	1.07	0.00 (0.13)	34.0 (4.3)	24.3
#10a	299 ± 1	48	GL6	7.83	7.89	0.575	0.0100	628 (67)	7.3	1.13	0.00 (0.03)	33.0 (3.5)	33.0
#65a	299 ± 1	48	GL6	7.19	7.51	0.575	0.0100	686 (16)	7.3	1.05	0.00 (0.06)	30.0 (0.7)	32.9
#10b	299 ± 1	48	GL6	7.36	8.14	1.167	0.0210	820 (30)	7.3	1.06	0.01 (0.04)	49.9 (1.8)	50.0
#10d	299 ± 1	48	GL6	7.62	8.42	2.362	0.0430	1206 (47)	7.3	1.08	0.00 (0.01)	64.8 (2.5)	79.9
#34c	200 ± 2	45	GL6	6.43	6.01	0.292	0.0050	743 (51)	6.1	1.05	0.15 (0.68)	13.5 (0.9)	13.3
#33a	200 ± 1	50	GL6	7.65	8.24	0.575	0.0100	1039 (52)	6.1	1.07	0.00 (0.05)	19.2 (1.0)	18.2
#34d	200 ± 2	45	GL6	7.93	8.08	0.575	0.0100	1081 (42)	6.1	1.04	0.00 (0.08)	18.4 (0.7)	18.2
#34a	200 ± 2	45	GL6	6.35	7.06	1.167	0.0210	1489 (50)	6.1	1.03	0.00 (0.02)	26.7 (0.9)	27.6
#34b	200 ± 2	45	GL6	7.79	6.82	2.362	0.0420	1853 (58)	6.1	1.02	0.00 (0.02)	41.7 (1.3)	44.6
#57a	197 ± 4	51	HGL6-1	5.34	6.73	4.424	0.0760	1883 (39)	6.0	1.04	0.00 (0.00)	68.8 (1.4)	67.4
#57c	197 ± 4	51	HGL6-1	5.8	5.96 *	10.527	0.1720	2130 (47)	6.0	1.04	0.00 (0.01)	114.6 (2.5)	115.1
#60a	122	48	HGL6-3	7.21	7.21	0.122	0.0016	702 (60)	4.8	1.02	<0.01	5.4 (0.5)	4.9
#61a	121 ± 1	48	HGL6-3	6.56	7.01	0.237	0.0030	1383 (77)	4.8	1.02	<0.01	5.3 (0.3)	5.8
#58b	122 ± 1	48	HGL6-1	6.03	6.01	0.435	0.0057	2088 (64)	4.8	1.04	0.00 (0.08)	6.5 (0.2)	7.3
#58a	122 ± 1	48	HGL6-1	5.47	6.02	0.642	0.0089	2518 (48)	4.8	1.05	0.00 (0.03)	8.2 (0.2)	8.9
Experiments conducted at T=1000 °C													
#74d	200 ± 1	48	HGL6-3	4.19	4.06	0.292	0.0049	969 (22)	6.3	1.09	0.03 (0.29)	10.1 (0.2)	8.2
#70a	200 ± 1	48	HGL6-3	4.65	5.30	0.575	0.0097	1807 (23)	6.3	1.04	0.30 (0.35)	10.7 (0.1)	11.1
#81a	198 ± 3	60	HGL6-5	4.55	4.79	0.575	0.0097	1745 (19)	6.3	1.10	0.11 (0.19)	11.0 (0.1)	11.1
#81b	198 ± 3	60	HGL6-5	4.95	5.10	1.167	0.0201	2569 (33)	6.3	1.08	0.10 (0.09)	15.1 (0.2)	16.8
#74c	200 ± 1	48	HGL6-3	4.15	4.29	2.362	0.0415	2139 (143)	6.3	1.11	0.00 (0.02)	35.7 (2.4)	27.5

The measured uncertainties (1σ) are shown in parenthesis.

[a] Total Cl molality in fluid (mol/kg H_2O)

[b] $X_{NaCl}= n_{NaCl}/ (n_{NaCl}+ n_{H2O})$ present calculated equilibrium fluid compositions; n= number of moles of each component

[c] H_2O solubility (as X_{H2O}=1 in the fluid) in the melt used for mass balance calculation according to Papale et al. (2006)

[d] A/NK= molar $Al_2O_3/(Na_2O + K_2O)$

[e] The ratios of HCl/NaCl in the fluid derived by mass balance of glass compositions (see section 4.1 for detail)

[f] The calculated Cl partition coefficients between fluid and melt obtained from the empirical equation.

Table 3. Experimental run conditions and initial Cl concentrations in the aqueous fluid and melt for the CO_2-bearing system

Run no.	P (MPa)	Run duration (h)	Starting glass	Glass (mg)	Solution (mg)	CO_2 (mg)[a]	Total mCl[b]	X_{NaCl}[c]	X_{CO2}[c]	Cl in melt (ppm)	Wt% H_2O in melt[d]	Wt% CO_2 in melt[d]	A/NK[e]	HCl/NaCl in fluid[f]	$D_{Cl}^{fluid/melt}$	$D_{Cl}^{fluid/melt}$ (modeled)[g]
Experiments conducted at T=850 °C																
#11a	299 ± 1	48	GL6	7.69	7.94	0.97	0.603	0.0100	0.052	713 (36)	7.0	0.0245	1.07	0.00 (0.09)	26.6 (1.3)	25.8
#11b	299 ± 1	48	GL6	7.92	7.62	1.71	0.658	0.0110	0.093	858 (53)	6.8	0.0394	1.07	0.00 (0.03)	21.9 (1.4)	21.8
#11c	299 ± 1	48	GL6	8.08	8.07	2.78	0.722	0.0110	0.135	1028 (34)	6.6	0.0527	1.04	0.01 (0.06)	17.9 (0.6)	17.7
#65c	299 ± 1	48	HGL6-3	6.80	6.95	3.81	0.912	0.0130	0.2	1458 (34)	6.3	0.0703	1.08	0.04 (0.06)	13.5 (0.3)	14.4
#11d	299 ± 1	48	GL6	7.95	8.01	5.11	0.954	0.0130	0.225	1702 (61)	6.1	0.0763	1.04	0.05 (0.08)	11.3 (0.4)	12.6
#65b	299 ± 1	48	HGL6-3	7.01	7.11	4.74	1.167	0.0160	0.234	1865 (45)	6.1	0.0780	1.07	0.04 (0.05)	12.3 (0.3)	13.8
#65d	299 ± 1	48	HGL6-3	7.75	7.19	5.6	1.508	0.0190	0.266	2246 (47)	5.9	0.0851	1.06	0.05 (0.06)	12.1 (0.3)	13.0
#33d	200 ± 1	50	GL6	8.12	7.96	0.62	0.586	0.0100	0.034	1325 (34)	6.0	0.0080	1.06	0.00 (0.07)	13.9 (0.4)	15.5
#72*	200 ± 1	24	HGL6-3	4.89	4.47	0.90	0.658	0.0106	0.083	1145 (112)	5.7	0.0184	1.06		16.3 (1.6)	
#33c	200 ± 1	50	GL6	7.82	7.61	1.62	0.658	0.0100	0.087	1702 (32)	5.7	0.0194	1.02	0.10 (0.16)	10.6 (0.2)	12.0
#73b	200 ± 1	94	HGL6-3	4.81	5.12	1.12	0.658	0.0100	0.089	1511 (24)	5.7	0.0197	1.06	0.08 (0.12)	12.0 (0.2)	12.0
#33b	200 ± 1	50	GL6	8.39	8.07	3.11	0.722	0.0110	0.148	2162 (53)	5.5	0.0305	1.02	0.10 (0.16)	7.8 (0.2)	9.1
#69a	200 ± 1	49	HGL6-3	5.68	5.95	3.39	0.912	0.0120	0.203	2497 (37)	5.2	0.0395	1.03	0.10 (0.12)	7.5 (0.1)	7.8
#57b	197 ± 4	51	HGL6-3	7.28	7.18	5.28	0.954	0.0120	0.248	2462 (116)	5.0	0.0462	1.02	0.19 (0.15)	7.1 (0.3)	6.2
#73a	200 ± 1	94	HGL6-3	4.81	5.15	3.67	1.167	0.0150	0.243	2753 (54)	5.0	0.0456	1.01	0.14 (0.09)	7.9 (0.2)	7.3
#77b	199 ± 1	50	HGL6-3	4.60	4.10	1.23	1.368	0.0210	0.122	2177 (63)	5.6	0.0257	1.07	0.02 (0.06)	15.8 (0.5)	15.5
#77a	199 ± 1	50	HGL6-3	4.42	4.08	2.88	1.508	0.0194	0.246	2703 (68)	5.0	0.0457	1.04		two-phase	
#78b	205	53	HGL6-5	4.65	4.08	1.01	2.668	0.0420	0.107	2366 (173)	5.6	0.0230	1.10	0.03 (0.04)	28.4 (2.1)	25.9
#78a	205	53	GL6	5.65	4.33	2.18	3.028	0.0421	0.201	2676 (42)	5.2	0.0385	1.02		two-phase	
#58c	122 ± 1	48	HGL6-3	7.28	6.90	0.98	0.122	0.0017	0.058	812 (50)	4.6	0.0067	1.05	<0.01	3.9 (0.2)	3.7
#60b	122	48	HGL6-3	7.35	6.97	1.81	0.122	0.0016	0.101	936 (42)	4.5	0.0113	1.03	<0.01	2.9 (0.1)	3.1
#64a	119 ± 5	95	HGL6-3	6.63	6.95	2.81	0.125	0.0015	0.148	978 (32)	4.3	0.0162	1.06	<0.01	2.6 (0.1)	2.5
#64b	119 ± 5	95	HGL6-3	6.76	6.92	3.92	0.171	0.0021	0.196	1320 (114)	4.1	0.0209	1.05	<0.01	2.3 (0.2)	2.1
#68	120 ± 5	168	HGL6-3	6.74	6.33	4.51	0.171	0.0020	0.235	1435 (79)	4.0	0.0246	1.04	<0.01	1.9 (0.1)	1.8
Experiments conducted at T=1000 °C																
#74a	200 ± 1	48	HGL6-3	4.32	5.06	1.06	0.658	0.0101	0.085	2178 (57)	5.9	0.0198	1.08	0.04 (0.12)	8.2 (0.2)	7.7
#70c	200 ± 1	48	HGL6-3	4.79	5.07	1.94	0.722	0.0100	0.145	2782 (34)	5.6	0.0318	1.00	0.71 (0.71)	5.9 (0.1)	5.6
#70d	200 ± 1	48	HGL6-3	5.25	5.11	3.03	0.954	0.0121	0.211	3654 (37)	5.2	0.0432	0.98	0.52 (0.47)	5.0 (0.1)	4.6
#81c	198 ± 3	60	HGL6-5	5.40	4.38	2.43	3.028	0.0403	0.215	4012 (368)	5.2	0.0436	0.88		two-phase	

The measured uncertainties (1σ) are shown in parenthesis. * Experiment Run#72 was conducted at 820 °C

[a] The amount of CO_2 added in the starting fluid was calculated based on the anhydrous oxalic acid decomposition reaction: $H_2C_2O_4$=2*CO2 + H_2

[b] Total Cl molality in fluid (mol/kg H_2O)

[c] $X_{NaCl}=n_{NaCl}/(n_{NaCl}+n_{H2O}+n_{CO2})$ and $X_{CO2}=n_{CO2}/(n_{NaCl}+n_{H2O}+n_{CO2})$ present calculated equilibrium fluid compositions; n= number of moles of each component

[d] Wt% H_2O and CO_2 were calculated using a solubility model for H_2O + CO_2 fluid mixture (i.e. $X_{H2O}=1-X_{CO2}$) according to Papale et al. (2006)

[e] A/NK= molar $Al_2O_3/(Na_2O + K_2O)$

[f] The ratios of HCl/NaCl in the fluid derived by mass balance of glass compositions (see section 4.1 for detail)

[g] The calculated Cl partition coefficients between fluid and melt obtained from the empirical equation.

Table S1. Major element compositions of the run product glasses form the CO_2-free experiments

Run no.	n	SiO_2	SD	Al_2O_3	SD	Na_2O	SD	K_2O	SD	Total	SD	A/NK	n	Cl	SD	H_2O [a]	H_2O [b]
300 MPa, 850 °C																	
#10c	32	72.48	0.44	11.69	0.21	6.63	0.15	0.03	0.01	90.81	0.44	1.070	84	0.0315	0.0040	9.17	7.3
#10a	33	72.17	0.90	11.83	0.43	6.36	0.37	0.02	0.01	90.37	0.58	1.128	44	0.0628	0.0067	9.58	7.3
#65a	17	72.43	0.30	11.63	0.18	6.69	0.12	0.05	0.01	90.81	0.40	1.051	19	0.0686	0.0016	9.14	7.3
#10b	32	72.12	0.34	11.78	0.13	6.71	0.26	0.05	0.01	90.74	0.38	1.062	33	0.0820	0.0030	9.20	7.3
#10d	54	72.16	0.52	11.86	0.24	6.61	0.21	0.06	0.01	90.85	0.39	1.083	47	0.1206	0.0047	9.06	7.3
200 MPa, 850 °C																	
#34c	27	74.05	0.44	11.73	0.11	6.93	0.15	0.03	0.01	92.55	0.50	1.054	20	0.0743	0.0051	7.39	6.1
#33a	15	73.47	0.46	11.90	0.13	6.76	0.10	0.05	0.01	92.19	0.47	1.065	22	0.1039	0.0052	7.73	6.1
#34d	29	73.79	0.46	11.67	0.20	6.79	0.20	0.04	0.01	92.30	0.59	1.041	24	0.1081	0.0042	7.62	6.1
#34a	29	74.1	0.63	11.46	0.17	6.73	0.19	0.05	0.01	92.34	0.81	1.031	24	0.1489	0.0050	7.54	6.1
#34b	45	73.92	0.50	11.53	0.14	6.83	0.12	0.06	0.01	92.34	0.55	1.019	27	0.1853	0.0058	7.52	6.1
#57a	27	73.95	0.35	12.39	0.19	7.16	0.12	0.10	0.01	93.60	0.40	1.042	23	0.1883	0.0039	6.25	6.0
#57c	25	74.21	0.38	12.56	0.19	7.33	0.14	0.02	0.01	94.12	0.40	1.040	33	0.2130	0.0047	5.72	6.0
120 MPa, 850 °C																	
#60a	27	74.75	0.44	12.28	0.190	7.300	0.14	0.05	0.02	94.37	0.50	1.019	36	0.0702	0.0060	5.58	4.8
#61a	31	74.76	0.42	12.24	0.210	7.250	0.17	0.07	0.01	94.31	0.46	1.020	35	0.1383	0.0077	5.58	4.8
#58b	28	74.90	0.59	12.52	0.170	7.240	0.18	0.11	0.01	94.77	0.71	1.040	16	0.2088	0.0064	5.07	4.8
#58a	27	74.61	0.46	12.52	0.200	7.160	0.16	0.14	0.01	94.43	0.41	1.048	19	0.2518	0.0048	5.38	4.8
200 MPa, 1000 °C																	
#74d	22	72.75	0.34	12.10	0.15	6.75	0.20	0.03	0.01	91.63	0.45	1.086	21	0.0969	0.0022	8.29	6.3
#70a	16	72.35	0.59	12.32	0.16	7.16	0.17	0.05	0.01	91.87	0.85	1.042	21	0.1807	0.0023	7.99	6.3
#81a	9	72.35	0.44	12.48	0.13	6.87	0.09	0.04	0.01	91.74	0.54	1.101	15	0.1745	0.0019	8.12	6.3
#81b	11	72.07	0.35	12.57	0.11	7.04	0.08	0.05	0.01	91.73	0.39	1.079	15	0.2569	0.0033	8.07	6.3
#74c	25	72.11	0.47	12.06	0.13	6.55	0.35	0.08	0.01	90.80	0.73	1.111	24	0.2139	0.0143	9.03	6.3

All data are shown in wt% except Cl (in ppm) and are analyzed by microprobe analysis
n: number of analysis by EPMA
[a] cH_2O=100-(Total-cCl/70.9*16)
[b] H_2O concentrations according to Papale et al. (2006)

Table S2. Major element compositions of the run product glasses from the CO_2-bearing experiments

Run no.	n	SiO_2	SD	Al_2O_3	SD	Na_2O	SD	K_2O	SD	Total	SD	A/NK	n	Cl	SD	H_2O [a]	H_2O [b]	CO_2 [b]
300 MPa, 850 °C																		
#11a	52	72.01	1.07	11.76	0.24	6.64	0.29	0.04	0.01	90.44	1.32	1.072	27	0.0713	0.0036	9.50	7.0	0.0245
#11b	43	73.55	0.81	11.68	0.24	6.59	0.23	0.04	0.01	91.83	0.90	1.074	37	0.0858	0.0053	8.10	6.8	0.0394
#11c	24	73.4	0.88	11.63	0.14	6.78	0.17	0.06	0.01	91.83	1.08	1.037	32	0.1028	0.0034	8.09	6.6	0.0527
#65c	19	73.12	0.53	12.31	0.26	6.91	0.13	0.06	0.01	92.39	0.40	1.076	19	0.1458	0.0034	7.50	6.3	0.0703
#11d	46	73.76	0.67	11.97	0.25	7.00	0.19	0.05	0.02	92.76	0.72	1.035	48	0.1702	0.0061	7.11	6.1	0.0763
#65b	20	73.21	0.33	12.25	0.24	6.95	0.12	0.06	0.01	92.47	0.34	1.065	19	0.1865	0.0045	7.39	6.1	0.0780
#65d	13	73.11	0.29	12.34	0.15	7.06	0.10	0.06	0.01	92.58	0.22	1.056	15	0.2246	0.0047	7.25	5.9	0.0851
200 MPa, 850 °C																		
#33d	22	73.38	0.47	11.92	0.17	6.79	0.1	0.05	0.02	92.14	0.54	1.062	52	0.1325	0.0034	7.76	6.0	0.0080
#72	10	73.24	0.43	12.16	0.16	6.98	0.13	0.04	0.01	92.42	0.61	1.056	33	0.1145	0.0112	7.49	5.7	0.0184
#33c	21	73.49	0.73	11.77	0.17	6.99	0.13	0.06	0.01	92.30	0.79	1.018	39	0.1702	0.0032	7.57	5.7	0.0194
#73b	11	73.42	0.37	12.26	0.11	7.00	0.14	0.05	0.01	92.73	0.52	1.059	15	0.1511	0.0024	7.15	5.7	0.0197
#33b	19	73.68	0.6	11.89	0.1	7.03	0.17	0.05	0.01	92.65	0.54	1.023	39	0.2162	0.0053	7.18	5.5	0.0305
#69a	16	74.27	0.31	12.22	0.19	7.19	0.17	0.05	0.01	93.73	0.38	1.028	12	0.2497	0.0037	6.08	5.2	0.0395
#57b	26	74.97	0.42	12.53	0.25	7.44	0.13	0.06	0.01	95.00	0.49	1.019	34	0.2462	0.0116	4.81	5.0	0.0462
#73a	9	73.78	0.23	12.26	0.18	7.35	0.09	0.06	0.01	93.44	0.30	1.009	12	0.2753	0.0054	6.35	5.0	0.0456
#77b	25	73.40	0.52	12.16	0.17	6.88	0.30	0.06	0.01	92.50	0.52	1.069	20	0.2177	0.0063	7.33	5.6	0.0257
#77a	20	74.09	0.37	12.24	0.31	7.09	0.14	0.06	0.01	93.48	0.38	1.043	17	0.2703	0.0068	6.31	5.0	0.0457
#78b	10	72.61	0.89	12.57	0.52	6.92	0.28	0.07	0.01	92.17	0.23	1.096	20	0.2366	0.0173	7.65	5.6	0.0230
#78a	7	73.64	0.72	12.02	0.37	7.12	0.15	0.08	0.01	92.85	0.38	1.019	17	0.2676	0.0042	6.94	5.2	0.0385
120 MPa, 850 °C																		
#58c	27	75.48	0.53	12.65	0.19	7.27	0.14	0.05	0.01	95.46	0.69	1.053	16	0.0812	0.0050	4.48	4.6	0.0067
#60b	26	75.59	0.47	12.50	0.22	7.34	0.12	0.04	0.01	95.47	0.49	1.032	28	0.0936	0.0042	4.46	4.5	0.0113
#64a	13	75.26	0.37	12.39	0.18	7.09	0.13	0.04	0.01	94.78	0.44	1.058	19	0.0978	0.0032	5.14	4.3	0.0162
#64b	30	75.5	0.43	12.50	0.27	7.22	0.19	0.05	0.01	95.26	0.64	1.048	40	0.1320	0.0114	4.64	4.1	0.0209
#68	17	75.5	0.52	12.65	0.15	7.34	0.12	0.05	0.02	95.53	0.55	1.043	32	0.1435	0.0079	4.36	4.0	0.0246
200 MPa, 1000 °C																		
#74a	26	72.49	0.48	12.16	0.12	6.83	0.34	0.06	0.01	91.53	0.81	1.076	21	0.2178	0.0057	8.30	5.87	0.0198
#70c	13	73.55	0.29	12.4	0.14	7.54	0.09	0.04	0.01	93.54	0.34	0.996	24	0.2782	0.0034	6.24	5.56	0.0318
#70d	15	73.53	0.25	12.23	0.12	7.57	0.2	0.05	0.01	93.38	0.41	0.978	20	0.3654	0.0037	6.34	5.25	0.0432
#81c	15	72.77	0.88	12.42	0.15	8.51	0.28	0.09	0.01	93.78	1.22	0.881	13	0.4012	0.0368	5.91	5.24	0.0436

All data are shown in wt% except Cl (in ppm) and are analyzed by microprobe analysis
n: number of analysis by EPMA
[a] cH_2O=100-(Total-cCl/70.9*16)
[b] H_2O and CO_2 concentrations according to Papale et al. (2006)